Phosphoproteomic mapping reveals distinct signaling actions and activation of protein synthesis and muscle hypertrophy by Isthmin-1

Meng Zhao[1,2,3], Niels Banhos Danneskiold-Samsøe[1], Livia Ulicna[1], Quennie Nguyen[1], Laetitia Voilquin[1,2,3], David E. Lee[4,5], James P. White[4,5,6], Zewen Jiang[1,7,8], Nickeisha Cuthbert[1], Shrika Paramasivam[1], Ewa Bielczyk-Maczynska[2,3,9], Capucine Van Rechem[1], Katrin J. Svensson[1,2,3,*]

1. Department of Pathology, Stanford University School of Medicine, Stanford, CA, 94305, USA.
2. Stanford Diabetes Research Center, Stanford University School of Medicine, Stanford, CA, 94305, USA.
3. Stanford Cardiovascular Institute, Stanford University School of Medicine, CA, USA.
4. Duke Molecular Physiology Institute, Duke University School of Medicine, Durham, NC, USA.
5. Department of Medicine, Duke University School of Medicine, Durham, NC, USA.
6. Duke Center for the Study of Aging and Human Development, Duke University School of Medicine, Durham, NC, USA.
7. Department of Laboratory Medicine, University of California San Francisco, San Francisco, CA, USA
8. Diabetes Center, University of California San Francisco, San Francisco, CA, USA.
9. Division of Cardiovascular Medicine, Department of Medicine, Stanford University School of Medicine, Stanford, CA, USA.

[*] Corresponding author: Katrin J. Svensson. Email: katrinjs@stanford.edu

Abstract

The secreted protein Isthmin-1 (Ism1) mitigates diabetes by increasing adipocyte and skeletal muscle glucose uptake by activating the PI3K-Akt pathway. However, while both Ism1 and insulin converge on these common targets, Ism1 has distinct cellular actions suggesting divergence in downstream intracellular signaling pathways. To understand the biological complexity of Ism1 signaling, we performed phosphoproteomic analysis after acute exposure, revealing overlapping and distinct pathways of Ism1 and insulin. We identify a 53 % overlap between Ism1 and insulin signaling and Ism1-mediated phosphoproteome-wide alterations in ~ 450 proteins that are not shared with insulin. Interestingly, we find several unknown phosphorylation sites on proteins related to protein translation, mTOR pathway and, unexpectedly, muscle function in the Ism1 signaling network. Physiologically, Ism1 ablation in mice results in altered proteostasis, including lower muscle protein levels under fed and fasted conditions, reduced amino acid incorporation into proteins, and reduced phosphorylation of the key protein synthesis effectors Akt and downstream mTORC1 targets. As metabolic disorders such as diabetes are associated with accelerated loss of skeletal muscle protein content, these studies define a non-canonical mechanism by which this anti-diabetic circulating protein controls muscle biology.

Introduction

Hormonal signaling through protein phosphorylation is one of the most important post-translational modifications allowing for rapid changes in cellular metabolic states (Humphrey et al., 2015). Metabolic stressors such as diabetes or fasting can lead to pronounced physiologic and cellular adaptations in protein regulation (Powers et al., 2009). Consequently, pathologic conditions can result in muscle atrophy, a net loss of muscle mass, which is highly associated with morbidity (Cohen et al., 2015; Jackman and Kandarian, 2004). Muscle strength is reduced in individuals with insulin resistance and type 2 diabetes (Andersen et al., 2004; Park et al., 2007), and muscle weakness is even a diagnostic predictor of diabetes (Peterson et al., 2016). The mechanisms underlying this association have remained elusive, but it is plausible that factors derived from adipose tissue can contribute to muscle proteostasis. Identifying such molecular triggers of muscle metabolism could facilitate our efforts to develop pharmacological agents that improve muscle function and systemic metabolic health.

Skeletal muscle is the most abundant tissue in humans, representing up to half of the total mass in normal-weight individuals (Janssen et al., 2000). As a major organ for glycogen storage and insulin-mediated glucose uptake, skeletal muscle controls whole-body energy expenditure and nutrient homeostasis (Deshmukh, 2016; Shulman et al., 1990). Importantly, skeletal muscle also acts as a protein reservoir that is highly responsive to anabolic or catabolic hormonal stimulation, including growth hormone (GH) and insulin-like growth factor-1 (IGF-1), both of which stimulate muscle fiber size (hypertrophy) (Moro et al., 2016; Velloso, 2008). Muscle mass is balanced by pathways controlling protein synthesis and protein degradation. The most well-described anabolic signaling pathway that promotes protein synthesis requires Akt/mTORC1 signaling, which robustly induces muscle hypertrophy upon stimulation by growth factors or amino acids (Bodine et al., 2001; Glass, 2011; Lai et al., 2004). In both flies (Scanga et al., 2000) and mammals

(Edinger and Thompson, 2002), the PI3K-Akt pathway controls cell size by increasing protein synthesis at the level of translation initiation. Akt also inhibits the catabolic function of FoxO family members, which upon phosphorylation are no longer able to enter the nucleus and turn on the transcription of atrophy genes, including the E3 ubiquitin ligases MuRF1 and Atrogin-1 (Bodine et al., 2001; Bodine and Baehr, 2014; Gomes et al., 2001; Lecker et al., 1999).

We recently reported that the adipocyte-secreted protein Isthmin-1 (Ism1) improves glucose tolerance and insulin resistance by phosphorylating Akt^{S473}, which mediates increased adipose and skeletal muscle glucose uptake (Jiang et al., 2021). ISM1 adipose expression and circulating levels are elevated in mice and humans with obesity (Jiang et al., 2021; Ruiz-Ojeda et al., 2022), suggesting that the expression is under nutrient-sensing regulatory control. Intriguingly, Ism1 administration to mice simultaneously prevents hepatic lipid accumulation while increasing protein synthesis in hepatocytes (Jiang et al., 2021), demonstrating that Ism1 governs an anabolic pathway that is molecularly and functionally distinct from insulin. In the present study, we find that Ism1 induces specific Ism1-regulated phosphoproteome changes enriched for proteins controlling protein translation, mTOR signaling, and muscle function. Furthermore, we show that Ism1 is important to maintain skeletal muscle fiber size under fasting, thereby defining a non-canonical mechanism by which Ism1 controls muscle biology.

100 # Results

101 **Phosphoproteomics reveals overlapping and distinct pathways of Ism1 and insulin**

102 The PI3K-Akt pathway is a key pathway of convergence for ligands that activate receptor tyrosine
103 kinases (RTKs), including insulin (Humphrey et al., 2013; Luo et al., 2003; Zhao et al., 2020). We
104 recently identified Ism1 as an adipose-secreted protein that increases glucose uptake into fat and
105 muscle by potently activating PI3K-Akt signaling across a range of mouse and human cell types,
106 but unlike insulin, does not induce *de novo* lipogenesis (Jiang et al., 2021). Therefore, the extent
107 to which the entire Ism1-signaling network overlaps with insulin or whether other signaling nodes
108 are involved remains to be determined. Therefore, to increase our understanding of the signaling
109 divergence and obtain an unbiased, more complete view of the Ism1-induced signaling network,
110 we performed phosphoproteomics in the Ism1 and insulin-responsive 3T3-F442A cells. To
111 characterize the Ism1-induced phospho-signaling profile after acute treatment in cells, we used
112 phosphopeptide enrichment with TiO_2 followed by LC-MS/MS using Orbitrap Elite (Yue et al.,
113 2015; Zhou et al., 2008) (***Figure 1A***). Cells were starved overnight, followed by a 5-minute
114 treatment with 100 nM recombinant Ism1, or 100 nM insulin. As a negative control, bovine serum
115 albumin (BSA), a secreted protein in the same size range as Ism1, was used at 100 nM. Although
116 pAkt induction was more pronounced by insulin, we observed robust activation of pAkt 5 min post-
117 treatment with Ism1, and therefore selected this time point for our analysis (***Figure 1B***). The
118 proteomic experiments were performed in treatment groups of six biological replicates pooled as
119 duplicate samples for the proteomics analysis. In total, ~7700 raw MS precursor ions (peptides)
120 were acquired, resulting in the identification of unique phosphopeptides on >5000 proteins
121 (***Figure 1 - figure supplement 1***). Principal component analysis (PCA) demonstrates high
122 reproducibility between biological replicates and distinct separation of the Ism1- and insulin-
123 treated groups compared with each other and the albumin control (***Figure 1C***). Interestingly, we
124 identify overlapping and distinct Ism1 and insulin-specific phosphoproteome-wide alterations

upon acute stimulation, with BSA as control. First, there is a 53 % overlap between Ism1 and insulin signaling (***Figure 1D***). For example, insulin induces phosphorylation of 654 phosphosites, out of which 347 phosphosites are also phosphorylated or dephosphorylated by Ism1 (***Figure 1D***).

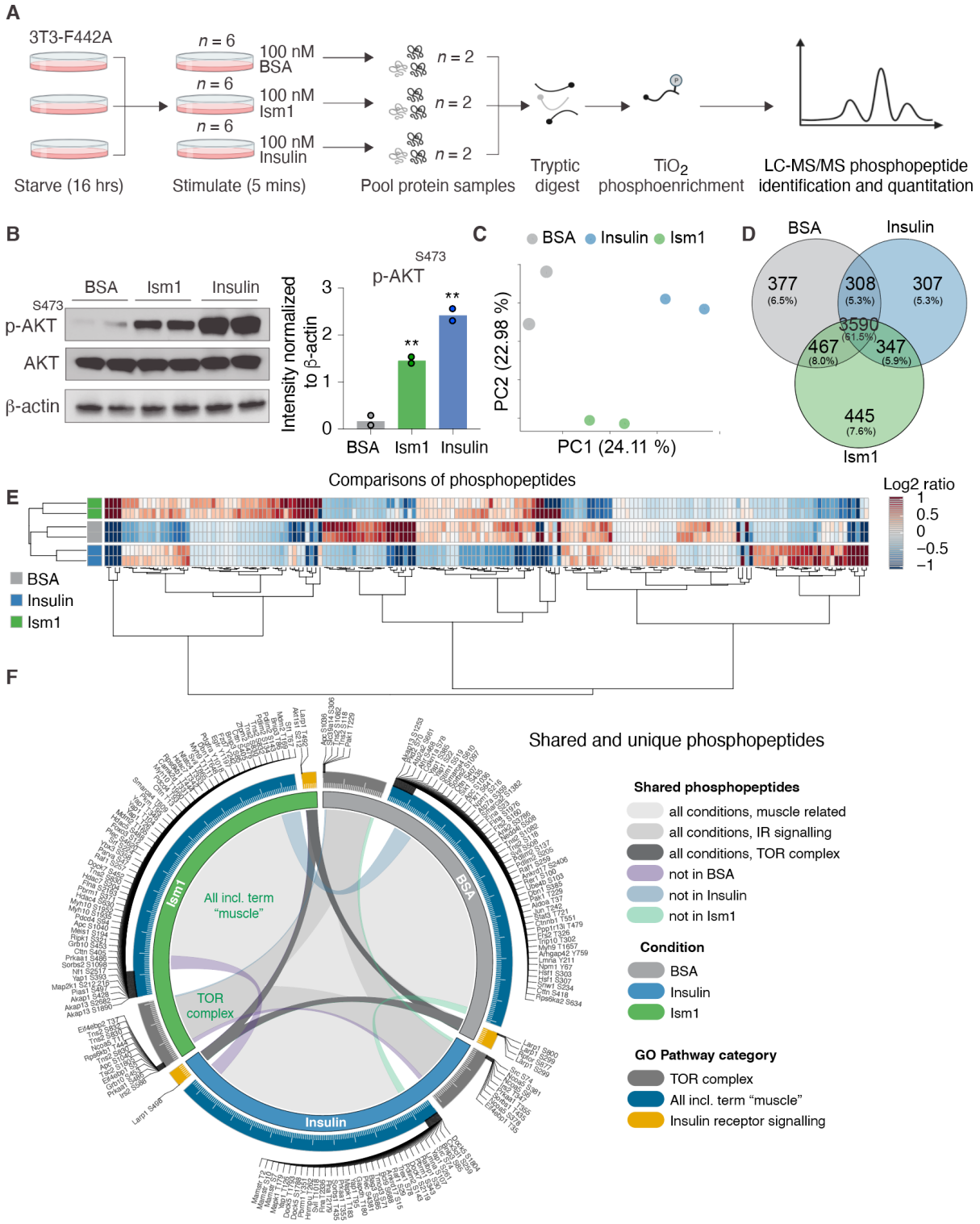

129 **Figure 1. Phosphoproteomics reveals overlapping and distinct pathways of Ism1 and insulin.** (A)
130 Experimental design of the untargeted phosphoproteomics analysis. 3T3-F442A cells were serum starved
131 for 16 hours and treated with 100 nM recombinant Ism1 or insulin for 5 minutes (*n* = 6 per group). Proteins
132 were extracted, trypsin digested, and fractionated. Phosphopeptides were enriched using TiO2
133 chromatography and phosphopeptides were analyzed with LC-MS/MS. (B) Western blot analysis of p-
134 AKT^{S473}, total AKT, and β-actin in cells treated with 100 nM bovine serum albumin (BSA), 100 nM Ism1, or
135 100 nM insulin for 5 minutes (*n* = 2 pooled from *n* = 6 per treatment group). P values are calculated by two-
136 tailed Student's t-test, *p < 0.05, **p < 0.01, ***p < 0.001.). (C) Protein intensity-based principal component
137 analysis (PCA) of the phosphoproteomic dataset. (D) Venn diagram of the phosphopeptides detected in
138 both replicates after BSA-, Ism1-, or insulin treatment. (E) Heatmap of differentially phosphorylated peptides
139 with 100 lowest significant p-values (adj. p < 0.05) from three comparisons displayed as log2 ratio (BSA vs.
140 Ism1, BSA vs. Insulin, and Insulin vs. Ism1). (F) Distribution diagram of shared and unique phosphosites
141 (detected in at least 1 sample) between treatments for selected GO pathways. Inner links in shades show
142 phosphosites detected in two or more treatment conditions. Gray shows phosphosites detected in all
143 samples; purple shows phosphosites detected in both Ism1 and insulin-treated cells; green shows
144 phosphosites detected in both BSA and insulin-treated cells; blue shows phosphosites detected in both
145 BSA and Ism1 treated cells. The middle ring displays GO pathway/pathway group with ticks indicating the
146 number of phosphopeptides. Large ticks indicate 50 phosphopeptides, and small ticks indicate 5
147 phosphopeptides. The outer ring displays gene symbols and the phosphosite exclusively detected in each
148 treatment. See also Figure 1—figure supplement 1, and Figure 1—source data 1, 2 and 3.
149

150 Remarkably, Ism1 causes changes in the phosphorylation status of 445 proteins compared with
151 BSA that are not shared with insulin and not previously described (***Figure 1D***). Groupwise
152 comparisons between treatments show phosphosites selectively regulated by the specific ligands
153 (adj. p value of < 0.05), many of which have not previously been identified (***Figure 1E***). Based on
154 the notion that Ism1 causes alterations in phosphorylation of a subset of proteins, while another
155 subset is shared with insulin, we next used GO analysis to discern cellular signaling pathways

156 associated with Ism1 or insulin. While Ism1 and insulin share the majority of phosphopeptides for
157 detected genes annotated to these GO terms, some phosphorylated residues could only be
158 identified in one condition (***Figure 1F***). Furthermore, we analyzed to which extent the
159 phosphorylation patterns overlapped between the Ism1 and insulin for genes belonging to the GO
160 terms "GO:0008286, insulin receptor signaling", "GO:0038201, TOR complex", and GO terms
161 including the word "muscle" (***Figure 1F***). Interestingly, we find that Ism1 exclusively alters the
162 phosphorylation status of proteins involved in the mTOR complex and muscle (***Figure 1F).*** These
163 overlapping and distinct signaling nodes may reflect the signaling networks underlying the cell-
164 specific responses.
165
166 **Phospho-specific mapping identifies an Ism1-induced signature consistent with protein**
167 **translation and muscle function**
168 To interrogate the Ism1-specific signal transduction pathway in more detail, we compared the
169 overlapping phosphopeptides clustered by functional GO pathway groups. Expectedly, insulin
170 induces robust phosphorylation of a subset of proteins, including the insulin receptor (IR). This
171 phosphoproteomic mapping shows that Ism1 does not induce the exact same targets in the insulin
172 pathway as insulin (***Figure 2A***), which is entirely consistent with our previous study using
173 phospho-tyrosine antibodies for the IR (Jiang et al., 2021). For example, only insulin
174 phosphorylates the InsR at Y1175/Y1163 while no significant phosphorylation is induced by Ism1
175 (***Figure 2B***). Interestingly, Ism1 induces phosphorylation of some of the same proteins as insulin,
176 including insulin receptor substrates Irs1 and Irs2, but with distinct phosphosite patterns. For
177 example, Irs2 was phosphorylated at T347 by insulin but at S588 by Ism1 (***Figure 1F, Figure 2 -***
178 ***figure supplement 1***). Therefore, Ism1 and insulin activate overlapping but distinct pathways,
179 which may account for some of the phenotypic and cell-type specific functions of Ism1. Similar
180 clustering for the mTOR and muscle pathways (***Figure 2C-D***) revealed several proteins regulated
181 only by insulin or only by Ism1. Both ligands induce phosphorylation of tuberin (Tsc2), a negative

182 regulator of mTOR with established roles in the control of protein synthesis (Inoki et al.,
183 2003)(Huang and Manning, 2008). Interestingly, insulin induces Tsc2^{S1806} phosphorylation
184 (***Figure 2E***), while Ism1 induces Tsc2^{S1421} phosphorylation (***Figure 2F***). Additionally, four other
185 phosphosites on Tsc2 are unchanged by Ism1. While the function of these specific phosphosites
186 of Tsc2 are understudied, our data suggest a direct regulation of mTOR activity, potentially
187 functionally distinct from insulin. Furthermore, Ism1 induced phosphorylation of several proteins
188 shown to regulate muscle growth and fiber size, such as Yes1 associated transcriptional regulator
189 (Yap1)^{T95} (Watt et al., 2015) (***Figure 2G***), Heat shock transcription factor 1 (Hsf1)^{S236}(Nishizawa
190 et al., 2013) (***Figure 2H),*** and FGF-receptor substrate 2 (Frs2)^{S327} (***Figure 2I***) (Chen and Friesel,
191 2009). Frs2 is also a lipid-anchored adapter protein and downstream mediator of signaling of
192 multiple receptor tyrosine kinases supporting the existence of a distinct Ism1 receptor (Zhou et
193 al., 2009). As protein translation is a critical downstream target of mTOR and the functionally
194 controls muscle growth, we next investigated the regulation of ribosomal targets that catalyze
195 protein synthesis. Interestingly, eukaryotic translation initiation factor 3 subunit A (Eif3), a
196 complex-subunit playing a major role in translation initiation (Ma et al., 2022), was phosphorylated
197 by insulin but not Ism1 (***Figure 2J***), while 60S ribosomal protein L12 (Rpl13) at S77 (***Figure 2K***)
198 and 40S ribosomal protein S13-1 (Rps13a) at S237 (***Figure 2L***) and Rps3a at S238 (***Figure 2M***)
199 were entirely dephosphorylated by both Ism1 and insulin. Lastly, ribosomal protein S6 kinase
200 alpha-5 (Rps6ka5), a known mTOR substrate (Chauvin et al., 2014) was phosphorylated by both
201 Ism1 and insulin at S375 (***Figure 2N***). These data conclude that Ism1 induces phosphorylation of
202 a specific set of proteins involved in mTOR signaling and proteostasis, while other phosphosites
203 are unchanged (***Figure 2O***).
204

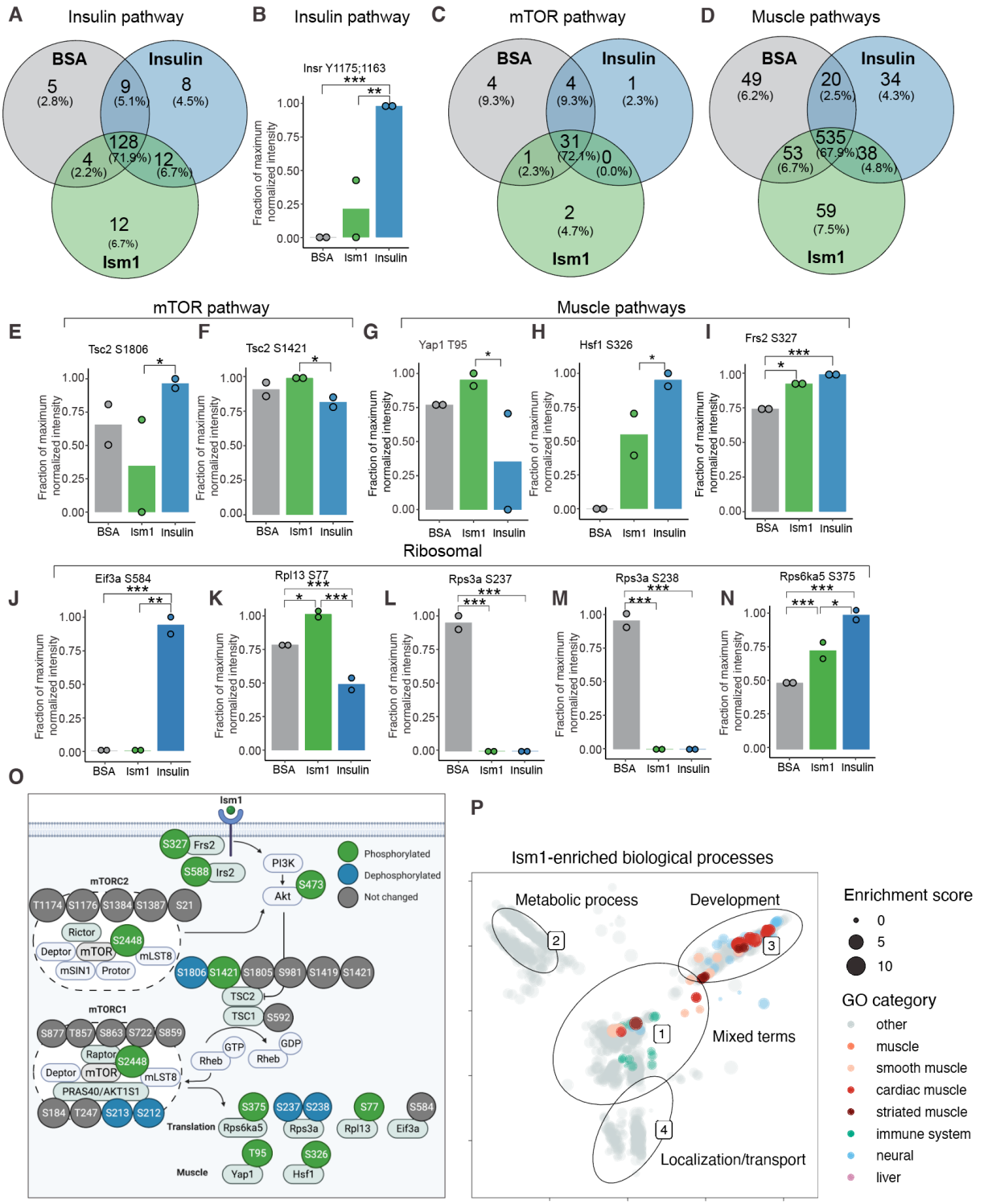

Figure 2. Phospho-specific mapping identifies an Ism1-induced signature consistent with protein translation and muscle function. (A) Venn diagram of shared and unique phosphosites between treatments for the GO pathways Insulin. (B) Abundance of InsR Y1175/1163 in cells treated with BSA, Ism1,

209 or insulin (*n* = 2). Individual comparisons between conditions across phosphopeptides was performed using
210 empirical Bayes statistics followed by adjustment for multiple testing using false discovery rate, *p < 0.05,
211 **p < 0.01, ***p < 0.001. The minimum normalized intensity across the dataset was subtracted from each
212 normalized data point, and phosphorylation was calculated as a fraction of the maximum value of all
213 samples for each phosphopeptide. Bars show mean ± SEM. C) Venn diagram of shared and unique
214 phosphosites between treatments for the GO pathways Insulin mTOR. D) Venn diagram of shared and
215 unique phosphosites between treatments for the GO pathways and Muscle. (E-N) Abundance of proteins
216 with indicated phosphosite in cells treated with BSA, Ism1, or insulin (*n* = 2). Individual comparisons
217 between conditions across phosphopeptides was performed using empirical Bayes statistics followed by
218 adjustment for multiple testing using false discovery rate, *p < 0.05, **p < 0.01, ***p < 0.001. The minimum
219 normalized intensity across the dataset was subtracted from each normalized data point, and
220 phosphorylation was calculated as a fraction of the maximum value of all samples for each phosphopeptide.
221 Bars show mean ± SEM. O) Ism1 signaling network in 3T3-F442A cells. Ism1 ligand stimulation triggers
222 activation of the PI3K/AKT pathway and the mTORC1 pathway which leads to changes in phosphorylation
223 status of multiple proteins involved in protein translation and muscle function. P) Pathway analysis of
224 enriched GO pathways in the Ism1 group versus BSA. Clusters are dominated by 1) mixed terms, 2)
225 metabolic process, 3) development and 4) localization/transport. Plotted GO terms all have P values <0.01
226 calculated using the classic Kolmogorov-Smirnov test. See also Figure 2—figure supplement 1, and Figure
227 2—source data 1 and 2.
228
229 To globally discern possible pathways activated by Ism1 and possible grouping of functional
230 effects, we conducted GO enrichment analysis using biological processes coupled with
231 visualization by semantic similarity. We found associations previously linked to Ism1, including
232 metabolic processes such as glucose and lipid metabolism (Jiang et al., 2021; Ruiz-Ojeda et al.,
233 2022), nervous system development (Osório et al., 2014; Pera et al., 2002), and the immune
234 system (Lam et al., 2022; Li et al., 2021; Valle-Rios et al., 2014; Wu et al., 2021) (***Figure 2P***).
235 Intriguingly, also here, we identify several pathways associated with muscle, skeletal muscle, and

236 cardiac muscle in the Ism1 treatment group (***Figure 2P***). These results show a broad regulation
237 of signatures indicating a role for Ism1 in muscle function.
238
239 **Ism1 induces mTOR-dependent protein synthesis in muscle cells**
240 Given the Ism1-induced muscle-signaling signature in 3T3-F442A cells and that the PI3K-Akt
241 pathway is known to promote anabolic programs in muscle cells (Edinger and Thompson, 2002),
242 muscle cell differentiation (Wilson and Rotwein, 2007), and skeletal muscle hypertrophy (Bodine
243 et al., 2001; Jaiswal et al., 2019), we next asked whether Ism1 induces anabolic cellular signaling
244 pathways in muscle cells. In differentiated C2C12 myotubes, Ism1 induces phosphorylation of
245 Akt^{S473} and ribosomal $S6^{S235/S236}$ starting at 5 min and remaining up to 4h (***Figure 3A***). The effect
246 of Ism1 on Akt signaling is robust but lower than that of the skeletal muscle hypertrophy hormone
247 insulin-like growth factor-1 (Igf1) (***Figure 3A-B***). Similarly, undifferentiated C2C12 myoblasts are
248 also responsive to Ism1 in a dose-dependent manner (***Figure 3C***). Notably, Ism1 treatment
249 induced a 2.5-fold increase in protein synthesis as determined by [^{35}S]-methionine incorporation
250 into proteins (***Figure 3D***). As expected, Igf1 treatment resulted in a 3-fold induction in protein
251 synthesis (***Figure 3D***), and the combined Igf1 and Ism1 treatment did not induce protein synthesis
252 further, suggesting that the maximal capacity of protein synthesis has been reached under these
253 conditions. Previous data showed that mTORC1/2 inhibition with rapamycin inhibits Ism1-induced
254 signaling in 3T3-F442A cells, demonstrating that intact mTOR activity is required for the signaling
255 capacity of Ism1 (Jiang et al., 2021). Importantly, low-dose rapamycin also inhibits Ism1-induced
256 protein synthesis, establishing that the functional effects are directly linked to the signaling
257 cascade induced by Ism1 (***Figure 3E***). These data align with the inhibitory effects of rapamycin
258 on muscle hypertrophy during anabolic conditions (Pallafacchina et al., 2002). In conclusion, Ism1
259 induces a signaling cascade that requires intact mTOR signaling to induce protein synthesis in
260 muscle cells.

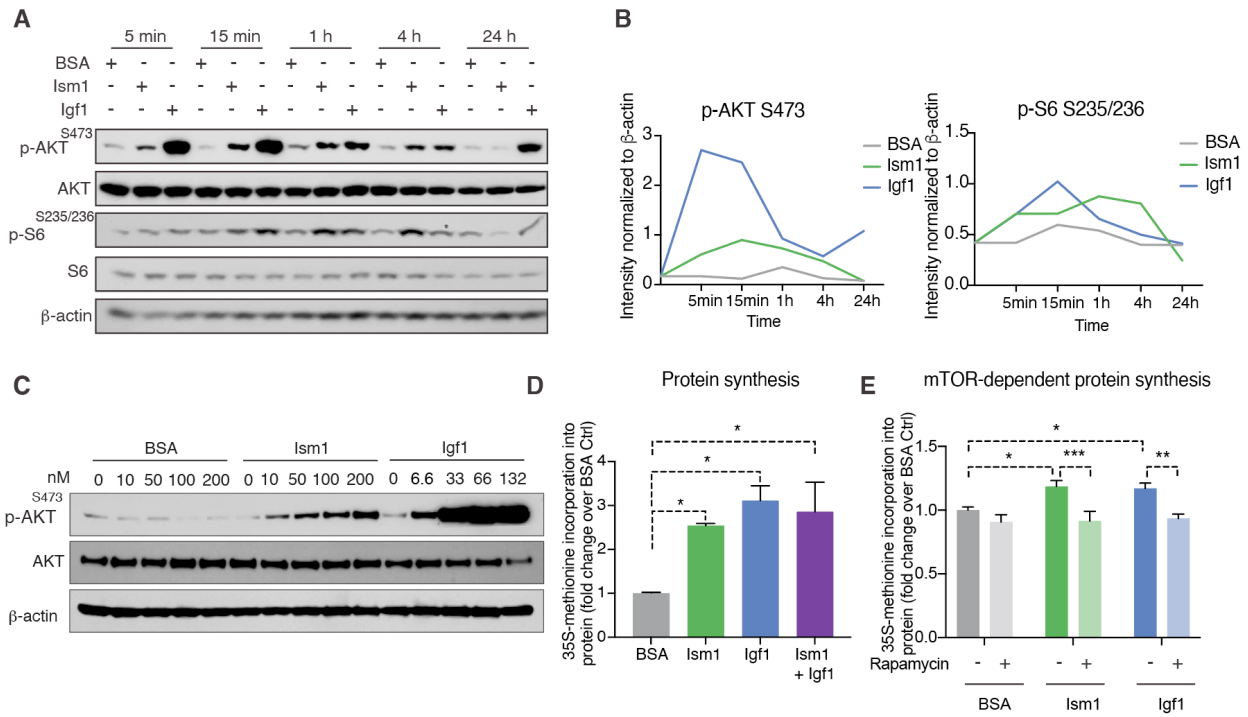

Figure 3. Ism1 induces mTOR-dependent protein synthesis in muscle cells. (A) Western blot analysis of p-AKT^{S473}, total AKT, p-S6$^{S235/}$236, total S6, and β-actin in C2C12 myotubes treated with 100 nM BSA, 100 nM Ism1, or 50 ng/ml Igf1. (B) Quantification of protein expression of p-AKT S473/ β-actin and p-S6 S235/236/β-actin. (C) Western blot analysis of p-AKT^{S473}, total AKT and β-actin in C2C12 myoblasts treated with indicated concentrations of BSA, Ism1, or Igf1 for 5 minutes. (D) Levels of protein synthesis measured by [35S]-methionine incorporation in C2C12 cells after 48 hours of indicated treatments (n = 3, one-way ANOVA, *p < 0.05, **p < 0.01, ***p < 0.001). (E) Levels of protein synthesis measured by [35S]-methionine incorporation in C2C12 cells with indicated treatments for 2 hours in the presence or absence of 100 nM mTOR inhibitor rapamycin (n = 3, two-way ANOVA, *p < 0.05, **p < 0.01, ***p < 0.001). Bar graphs show mean ± SEM. See also Figure 3—figure supplement 1 and 2, and Figure 3—source data 1 and 2.

Ism1 ablation results in reduced skeletal muscle fiber size and muscle strength

Skeletal muscle atrophy, a reduction in muscle mass, occurs when the protein degradation rate exceeds protein synthesis (Cohen et al., 2015; Jaiswal et al., 2019; Sandri et al., 2004). We previously showed that Ism1 controls glucose uptake into adipose tissue and skeletal muscle in

277 mice (Jiang et al., 2021), but the role of Ism1 in skeletal muscle function beyond glucose
278 regulation has not been studied. Ism1 is broadly expressed, including highly in adipose tissue and
279 blood (Jiang et al., 2021). By analyzing single-cell RNA sequencing data from murine skeletal
280 muscle (Baht et al., 2020), we find that Ism1 is not expressed in muscle precursors or mature
281 muscle cells (***Figure 3 - figure supplement 1***). Given the observed signaling action of Ism1 on
282 muscle cells, this indicated a non-cell-autonomous effect of Ism1 on muscle cells in a
283 physiological setting. Therefore, we next sought to determine whether whole-body ablation of
284 Ism1 in mice, in which blood levels of Ism1 are completely ablated (Jiang et al., 2021), resulted
285 in changes to skeletal muscle mass. To evaluate muscle atrophy, eight-week-old WT and Ism1-
286 KO mice were either fasted for 12 h or fasted followed by a 12 h re-feeding period (fed state)
287 (***Figure 3A***). As expected, at dissection, all fasted mice had a reduction in body weight compared
288 with fed mice (***Figure 3B***). Blood glucose levels were 150 mg/dl in the fed state, and < 80 mg/dl
289 in the fasted state (***Figure 3C***), but no differences were seen between genotypes. Under the same
290 conditions, quadriceps (***Figure 3D***), gastrocnemius (***Figure 3 - figure supplement 2***), as well as
291 tibialis (***Figure 3 - figure supplement 2***) muscles were harvested from mice under fed or fasted
292 states and analyzed for muscle fiber size. Muscle tissue morphology was similar between the
293 genotypes, but the muscle fiber size was notably smaller in the Ism1-KO quadriceps muscles
294 (***Figure 3D***). Remarkably, fiber size area quantifications showed that the Ism1-KO quadriceps
295 muscles demonstrate a robust shift in distribution to smaller muscle fiber size areas under both
296 fed and fasted conditions (***Figure 3E***). On average, loss of Ism1 significantly reduces the cross-
297 sectional area by 40 % in the fed state and > 20 % in the fasted state (***Figure 3F***). Given that the
298 Ism1 phenotype was more pronounced under the fed state, we next evaluated the effect of Ism1
299 ablation on muscle function. While the heart weights (***Figure 3 - figure supplement 2***), muscle
300 weights (***Figure 3 - figure supplement 2***), or total body weights (***Figure 3B***) of Ism1-KO mice
301 were not significantly different from WT, the reduction in muscle fiber size is associated with

302 impaired muscle force grip strength (***Figure 3G***). In conclusion, these results show that Ism1

303 ablation leads to smaller skeletal muscle fiber size and loss of muscle strength.

304

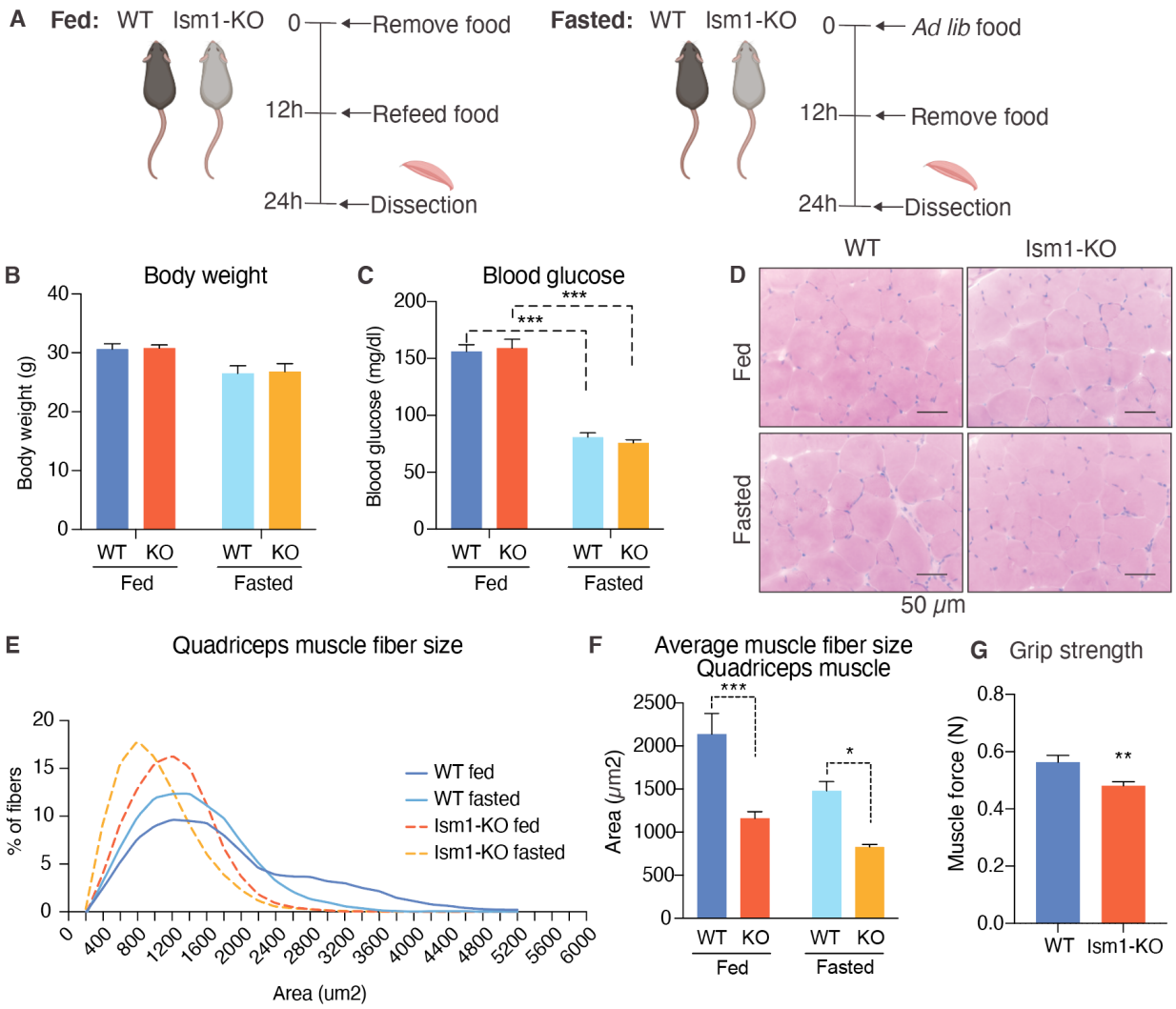

305

306 **Figure 4. Ism1 ablation results in reduced skeletal muscle fiber size and muscle strength.** (A)

307 Schematic description of the fasting and feeding protocol. (B) Body weights of WT and Ism1-KO mice in

308 the fed or fasted groups (WT fed, n = 3; Ism1-KO fed, n = 3; WT fasted, n = 3; Ism1-KO fasted, n = 3, two-

309 way ANOVA). (C) Blood glucose level in fed and fasted mice before dissection (WT fed, n = 3; Ism1-KO

310 fed, n = 3; WT fasted, n = 3; Ism1-KO fasted, n = 3, two-way ANOVA, *$p < 0.05$, **$p < 0.01$, ***$p < 0.001$).

311 (D) H&E staining of mouse quadriceps muscles from WT and Ism1-KO mice in the fed or fasted groups

312 (scale bars: 50 μm). Images are representative examples of three mice showing similar results. (E) Fiber

313 size distribution of mouse quad muscles (WT fed, *n* = 3; Ism1-KO fed, *n*= 3; WT fasted, *n* = 3; Ism1-KO
314 fasted, *n* = 3). Mean numbers of myotubes within the indicated area range is shown. (F) Quantification of
315 average muscle fiber area (WT fed, *n* = 3; Ism1-KO fed, *n* = 3; WT fasted, *n* = 3; Ism1-KO fasted, *n* = 3,
316 two-way ANOVA, *p < 0.05, **p < 0.01, ***p < 0.001) performed in a blinded fashion by two independent
317 investigators. This experiment was repeated using two independent cohorts of mice. (G) Grip strength
318 measured by muscle force (*N*) in WT and Ism1-KO mice (WT, *n* = 15; Ism1-KO, *n* = 15). P values are
319 calculated by two-tailed Student's t-test, *p < 0.05, **p < 0.01, ***p < 0.001. Bar graphs show mean ± SEM.
320 See also Figure 4—source data 1.
321

322 **Ism1 ablation does not impair movement or mitochondrial biogenesis, or normal muscle**
323 **development**

324 Since Ism1 ablation causes mild muscle atrophy, we next investigated whether loss of Ism1 is
325 associated with a reduction in movement or muscle mitochondrial complex dependent
326 mitochondrial bioenergetics, as has been demonstrated for IR and IGF-1R (Bhardwaj et al., 2021).
327 Ambulatory activity (***Figure 5A***), respiratory exchange ratio (RER) (***Figure 5B***), energy
328 expenditure as measured by VO_2 consumption (***Figure 5C***), or food intake (***Figure 5D***) are
329 indistinguishable between WT and Ism1-KO mice. Furthermore, protein levels of the
330 mitochondrial complexes under fed and fasted conditions show no significant differences in any
331 of the mitochondrial OXPHOS complexes I, II, III, IV, or V (***Figure 5E-F***). These data are
332 consistent with the notion that the expression of the canonical regulator of mitochondrial
333 biogenesis, *Ppargc1a* (*Pgc1*α) (Lin et al., 2002; Wu et al., 1999) is unchanged in quadriceps
334 muscle tissues from the Ism1-KO mice (***Figure 5G***). General muscle markers, including the
335 myosin heavy chain proteins *Myh1*, *Myh2*, *Myh4*, and *Myh7* were not altered under fed conditions,
336 and only *Myh4* was reduced in the Ism1-KO mice under fasted conditions, suggesting that muscle
337 differentiation is largely unaffected by Ism1 ablation and that the major role is in regulating
338 hypertrophy in terminally differentiated muscle cells (***Figure 5H***). Taken together, these data

339 suggest that Ism1 regulates muscle fiber size and muscle strength without affecting the
340 expression of mitochondrial complexes or whole-body energy expenditure.
341

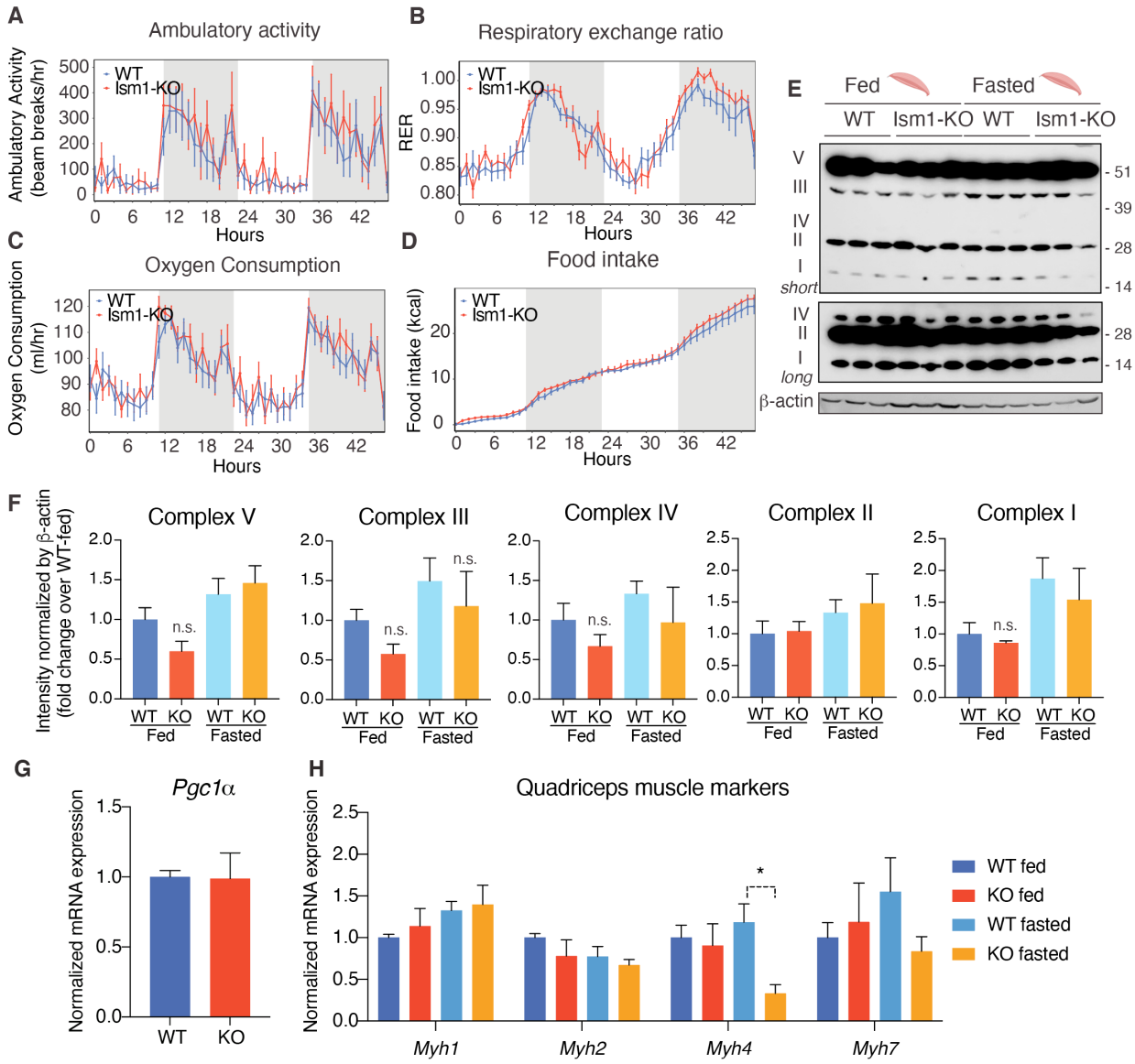

342

343 **Figure 5. Ism1 ablation does not impair movement, mitochondrial biogenesis, or normal muscle**
344 **development.** (A) Ambulatory activity (WT, *n* = 4; Ism1-KO, *n* = 4, ANOVA, *p < 0.05), (B) Respiratory
345 exchange ratio (RER) (WT, *n* = 4; Ism1-KO, *n*= 4, ANOVA, *p < 0.05), (C) Oxygen consumption (WT, *n* =
346 4; Ism1-KO, *n*= 4, ANCOVA, *p < 0.05), and (D) Food intake (WT, *n* = 4; Ism1-KO, *n*= 4, ANCOVA, *p <
347 0.05) in WT and Ism1-KO mice. (E) Levels of mitochondrial oxidative phosphorylation proteins in ETC

348 complexes (OXPHOS) from quadriceps muscles (WT fed, *n* = 3; Ism1-KO fed, *n*= 3; WT fasted, *n* = 3; Ism1-
349 KO fasted, *n* = 3) analyzed by Western blot. (F) Quantification of OXPHOS complexes (two-way ANOVA,
350 *p < 0.05, **p < 0.01, ***p < 0.001). (G) Relative gene expression analysis of *Pgc1*α in quadriceps muscle
351 from WT (*n* = 6) or Ism1-KO (*n* = 5) mice (two-tailed Student's t-test, *p < 0.05, **p < 0.01, ***p < 0.001).
352 (H) Relative gene expression analysis of *Myh1, Myh2, Myh4*, and *Myh7* in quadriceps muscle from WT fed
353 (*n* = 6) or Ism1-KO fed (*n* = 5) vs. WT fasted (*n* = 5) or Ism1-KO fasted (*n* = 5) mice (two-way ANOVA, *p
354 < 0.05, **p < 0.01, ***p < 0.001). Bar graphs show mean ± SEM. See also Figure 5—source data 1 and 2.
355

356 **Ism1-KO mice have defective skeletal muscle Akt and mTOR signaling and protein**
357 **synthesis**

358 To understand the underlying mechanism by which Ism1-KO mice develop smaller muscle fiber
359 size, we next asked whether Ism1 directly controls protein content in mice. Quadriceps muscles
360 from eight-week-old mice were harvested and analyzed for total protein content, demonstrating a
361 significant reduction in total protein content in the Ism1-KO mice compared with WT mice (***Figure***
362 ***6A***). Because muscle proteostasis is balanced by protein synthesis and degradation (Glass, 2011;
363 Jackman and Kandarian, 2004), we next tested the hypothesis that Ism1 is required for efficient
364 protein synthesis in mice by measuring *in vivo* [^{35}S]-methionine incorporation into proteins isolated
365 from quadriceps muscles (***Figure 6B***). WT and Ism1-KO mice were I.P. administered with [^{35}S]-
366 methionine for 2 hours, followed by protein precipitation, which demonstrates that loss of Ism1
367 results in a significant reduction in muscle protein synthesis in mice (***Figure 6C***). Furthermore,
368 under either fed or fasted conditions, muscles isolated from Ism1-KO mice have significantly
369 increased levels of atrophy genes FoxO1 (***Figure 6D***), the FoxO target genes *Cdkn1b*, *Eif4ebp1*,
370 and *Ctsl* (***Figure 6E***), and ubiquitin ligase *Fbxo30* compared with WT mice (***Figure 6F***). These
371 data suggest that Ism1 controls protein synthesis, and its loss is associated with elevated protein
372 degradation gene expression. Given that Ism1 activates the Akt pathway in myocytes *in vitro*, and
373 that loss of muscle-specific Akt1 and Akt2 leads to muscle atrophy (Jaiswal et al., 2019), we next

374 hypothesized that the mechanism behind the smaller muscle fiber size in the Ism1-KO mice is
375 due to reduced Akt pathway activity. Indeed, we found that phosphorylation of Akt^{S473}, $mTOR^{2448}$,
376 and ribosomal $S6^{S235/S236}$ are markedly decreased in Ism1-KO muscle compared with WT mice
377 under both fed and fast conditions, providing an explanation for the lower protein synthesis rate
378 (***Figure 6G***). Taken together, these results demonstrate that Ism1 is a circulating anabolic
379 regulator of protein synthesis and muscle function by maintaining high Akt activity and protein
380 synthesis in skeletal muscle. In conclusion, Ism1 is a circulating anabolic regulator of protein
381 synthesis and muscle function.

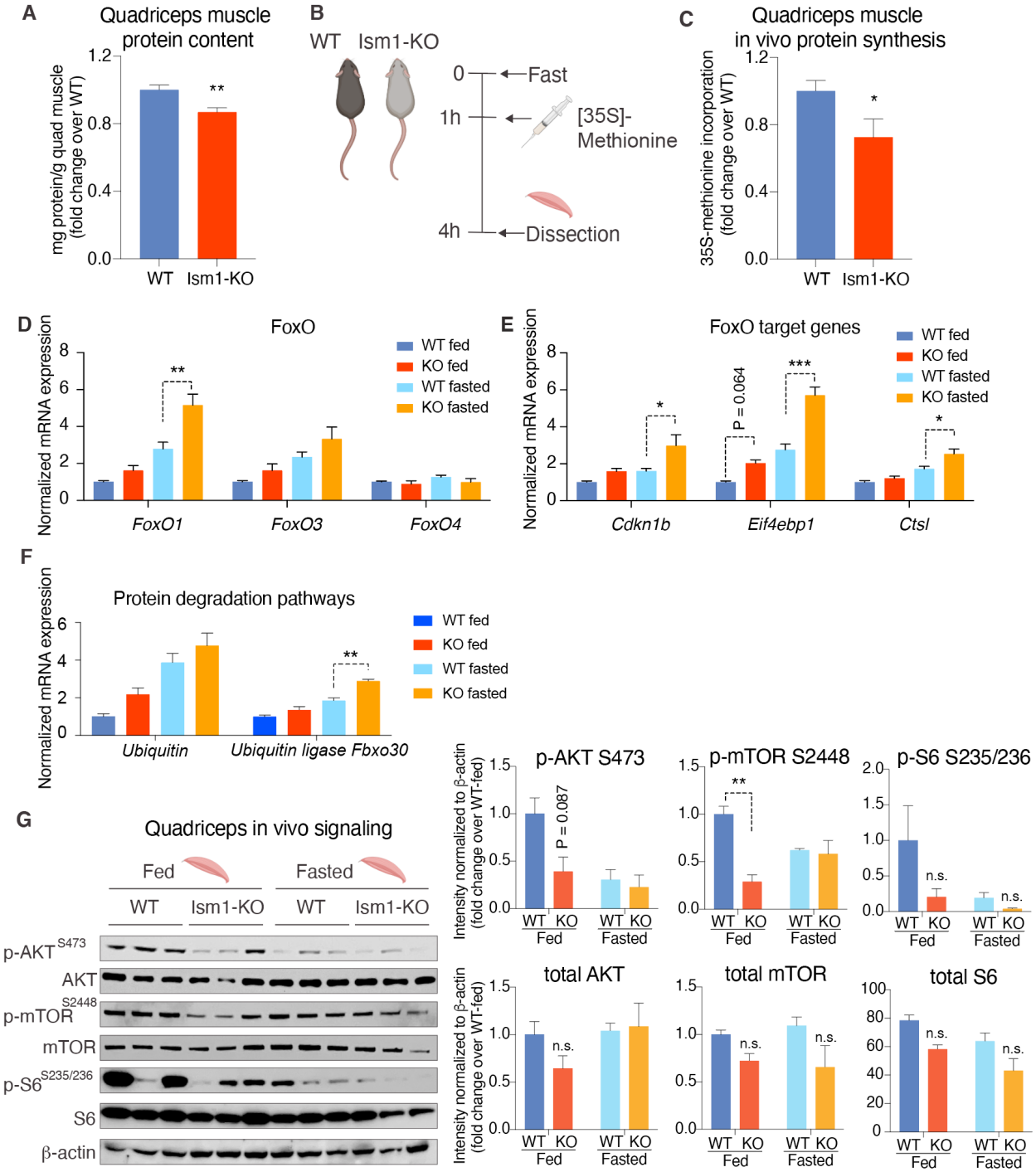

Figure 6. Ism1-KO mice have defective skeletal muscle protein synthesis and AKT-mTOR signaling. (A) Total protein content measured in WT and Ism1-KO quadriceps muscle expressed as mg protein/wet tissue weight in grams. (WT, n = 12; Ism1-KO, n = 9, two-tailed student's t-test *p < 0.05, **p < 0.01, ***p < 0.001). (B) Schematic description of the *in vivo* [35S]-methionine incorporation protocol. (C) *In vivo* protein

387 synthesis measured by [35S]-methionine incorporation in WT and Ism1-KO mice (WT, *n* = 12; Ism1-KO, *n*
388 = 9, two-tailed Student's t test, *p < 0.05, **p < 0.01, ***p < 0.001). Relative gene expression analysis of (D)
389 *FoxO* and (E) *FoxO* target genes *Cdkn1b, Eif4ebp1,* and *Ctsl* in quadriceps muscle from WT fed (*n* = 6) or
390 Ism1-KO fed (*n* = 5) vs. WT fasted (*n* = 5) or Ism1-KO fasted (*n* = 5) mice (two-way ANOVA, *p < 0.05, **p
391 < 0.01, ***p < 0.001). (F) Relative gene expression analysis of *Ubiquitin* and the ubiquitin ligase *Fbxo30* in
392 quadriceps muscle from WT fed (*n* = 6) or Ism1-KO fed (*n* = 5) vs. WT fasted (*n* = 5) or Ism1-KO fasted (*n*
393 = 5) mice. P values are calculated by two-way ANOVA, *p < 0.05, **p < 0.01, ***p < 0.001. Bar graphs show
394 mean ± SEM. (G) Western blot analysis and quantification of the *in vivo* levels of $pAKT^{S473}$, total AKT, p-
395 $mTOR^{S2448}$, total mTOR, $pS6^{S235/236}$, total S6, and β-actin in quadriceps muscles of WT and Ism1-KO mice
396 under fed and fasted conditions (WT fed, *n* = 3; Ism1-KO fed, *n* = 3, WT fasted, *n* = 3; Ism1-KO fasted, *n* =
397 3, two-way ANOVA, *p < 0.05, **p < 0.01, ***p < 0.001). Bar graphs show mean ± SEM. See also Figure
398 6—source data 1 and 2.
399
400
401
402
403
404
405
406
407
408
409
410
411
412

413 ## Discussion

414 Akt has an established role in enhancing muscle hypertrophy and function (Bodine et al., 2001;
415 Glass, 2011; Jaiswal et al., 2022, 2019; Lai et al., 2004; Mammucari et al., 2007; Wilson and
416 Rotwein, 2007). However, there is still a need to identify other hormonal and physiological
417 insulin/IGF-1 independent activators of Akt to avoid associated side effects such as hypoglycemia
418 when used therapeutically. We previously identified Ism1 as a secreted protein that activates Akt
419 in multiple cell types, including human skeletal muscle cells. Using radiolabeled glucose, we also
420 showed that Ism1 increases glucose transport into both adipose tissue and skeletal muscle (Jiang
421 et al., 2021). Several lines of evidence from the current study suggest that Ism1 also has an
422 important anabolic role in promoting skeletal muscle growth. Most importantly, Ism1 acts directly
423 on muscle cells to induce protein synthesis. Conversely, Ism1 ablation leads to lower skeletal
424 muscle fiber size and atrophy associated with lower Akt signaling and protein synthesis. Ism1-KO
425 mice have elevated levels of FoxO1 target genes consistent with increased protein degradation.
426 Therefore, Ism1 appears to be an important protein regulating metabolism during fed and fasted
427 conditions.
428
429 The signaling mechanism behind Ism1-induced muscle hypertrophy is not simply an activation of
430 the identical insulin/IGF-1-induced PI3K- Akt pathway. Across multiple cell types, Ism1 and insulin
431 share the pAkt and pS6 network but are seemingly segregated by the more robust activation of
432 $pAkt^{S473}$ seen with insulin, whereas Ism1 induces only a subset of shared Akt-induced insulin
433 targets. Interestingly, while Ism1 does not directly phosphorylate the IR/IGFRs, Ism1 does induce
434 phosphorylation of the insulin receptor substrate proteins (Irs), a feature that is shared with other
435 endocrine hormones. This phosphospecific regulation by distinct hormones can result in a diverse
436 range of functional outcomes (Yenush and White, 1997). For example, Irs1 phosphorylation at
437 S302, S307, S522 and S636/639 have been linked to insulin resistance (Um et al., 2004), but not

438 all hormones that phosphorylate those Irs sites induce insulin resistance, including FGF21
439 (Minard et al., 2016). These overlapping but distinct pathways may account for the Ism1's cell-
440 type specific functional outcomes and downstream transcriptional effects unique to Ism1.
441 Additionally, the phosphoproteomic mapping shows a distinct muscle signature specifically
442 induced by Ism1 and not by insulin. Among Ism1 downstream targets, we find phosphorylation of
443 proteins related to the mTOR pathway, ribosomal and muscle function, targets not previously
444 identified downstream of Ism1.
445
446 In this work, we observe a 60 % decrease in $pAkt^{S473}$ levels in the muscles of Ism1-KO mice,
447 which leads to a ~10 % reduction in muscle protein content. Our data is consistent with previous
448 reports using muscle-specific Akt-KO mice that demonstrate a 40% reduction in protein synthesis
449 upon complete ablation of Akt (Jaiswal et al., 2022). Furthermore, reduced Akt is associated with
450 skeletal muscle insulin resistance, in line with our previous observation that Ism1-KO mice fed a
451 high-fat diet are more insulin resistant (Jiang et al., 2021). To what extent the insulin resistance
452 in the Ism1-KO mice contributes to muscle function in obesity or during aging is an intriguing
453 question that remains to be answered in future work. Moreover, increasing protein synthesis while
454 suppressing protein degradation is important in a physiological setting, based on the findings that
455 only a combination of FoxO1 inhibition and mTORC1 activation can restore Akt-mediated muscle
456 loss (Jaiswal et al., 2022). This suggests that hormonal regulators of Akt activity could have
457 important biological functions because of Akt's dual role in regulating mTORC1 and the FoxO
458 genes. Here we used genetic and pharmacologic approaches to determine the role of Ism1 in
459 regulating protein synthesis, but it remains to be explored whether pharmacological Ism1
460 administration prevents protein degradation in the skeletal muscle. Additionally, upon muscle
461 hypertrophy, activated muscle precursors or satellite cells provide an additional mechanism for
462 muscle expansion (Hawke and Garry, 2001). A limitation of this study is that we did not investigate
463 whether Ism1 affects muscle regeneration. As IGF-1 induces the growth and differentiation of

464 satellite cells (Musarò et al., 1999), and HGF induces activation of cell cycle G_{Alert} (Rodgers et al.,
465 2017), it will be interesting to determine if Ism1 also activates skeletal muscle stem cells.
466 Identifying all physiological mechanisms that distinguish Ism1 from IGF-1 will aid in understanding
467 whether other yet unidentified pathways distinct from Akt and FoxO regulate proteostasis.
468
469 The physiological function of Ism1 in regulating muscle growth is expected given that Ism1
470 stimulates Akt, but it was somewhat unexpected that the lower muscle protein content and fiber
471 size did not lead to a significant loss of muscle mass. It remains to be determined what replaces
472 protein mass in the muscle of Ism1-KO mice, including water, glycogen stores, or lipids, which
473 could be regulated by Ism1. Notably, Ism1 itself is not expressed in muscle cells but only in other
474 cells, including adipocytes and immune cells. Circulating levels of human ISM1 using
475 immunoreactive ELISAs have been reported to be in the range of 1-50 ng/ml (Jiang et al., 2021;
476 Ruiz-Ojeda et al., 2022), consistent with mass spectrometry peptide analysis which estimates a
477 circulating ISM1 concentration of 17 ng/ml (Uhlén et al., 2019). The necessary circulating and
478 local Ism1 levels to maintain muscle fiber size or prevent fasting-induced muscle loss remain to
479 be determined. It is plausible that ISM1 levels are altered in response to fasting and feeding,
480 insulin resistance, or aging - conditions associated with temporary or chronic muscle loss
481 (Laurens et al., 2021; Perry et al., 2016; Roubenoff and Castaneda, 2001). A limitation of the
482 current study is that fasting, but not more severe atrophy conditions were studied. Long-term
483 studies ought to explore if pharmacological administration of Ism1 systemically or locally into the
484 muscle is sufficient to prevent muscle loss in more severe models of muscle loss. Nevertheless,
485 as aging impairs skeletal muscle protein synthesis and leads to muscle weakness and atrophy,
486 the current work has implications for multiple conditions, including diabetes- and age-induced
487 muscle atrophy.
488
489

490 ## Materials and Methods

491

492 **Animal studies.** Animal experiments were performed per procedures approved by the
493 Institutional Animal Care and Use Committee of the Stanford Animal Care and Use Committee
494 (APLAC) protocol number #32982. C57BL/6J mice were purchased from the Jackson Laboratory
495 (#000664). The Ism1-KO mice (C57BL/6J-Ism1^{em1Kajs}/J strain #036776, JAX) were generated
496 using the Ism1 floxed allele as described previously (Jiang et al., 2021). Unless otherwise stated,
497 mice were housed in a temperature-controlled (20-22°C) room on a 12-hour light/dark cycle. All
498 experiments were performed with sex- and age-matched, littermate male mice housed in groups
499 of five unless stated otherwise.

500

501 **Sample preparation for phosphoproteomics analysis.** The phosphoproteomics analysis was
502 performed using 3T3-F442A cells. Cells were cultured in DMEM/F12 medium with 10 % FBS/1 %
503 pen/strep until 80-100 % confluent. Following a 16 h starvation in serum-free DMEM/F12 medium,
504 cells were treated with PBS, 100 nM Ism1 or 100 nM insulin for 5 minutes (*N* = 6 per treatment
505 group, 10M cells/treatment). Following treatment, the medium was aspirated, and cells were
506 washed three times with ice-cold PBS while kept on ice. 1 ml ice-cold PBS supplemented with
507 complete mini protease inhibitors (#4693124001, Sigma-Aldrich, St. Louis, MO, USA) and
508 phosSTOP phosphatase inhibitors (#4906845001, Sigma-Aldrich, St. Louis, MO, USA) were
509 added to the cells that were immediately scraped down, pelleted at 14,000 *x* g for 10 min followed
510 by snap freezing. Cell pellets were kept at -80°C until analysis. Aliquots of the samples were used
511 to verify AKT^{S473} signaling induction by Ism1 and insulin by western blot. Six biological replicates
512 per treatment group were pooled into two replicates per treatment group for the
513 phosphoproteomics analysis. The phosphoproteomics analysis was performed at Northwestern
514 University Proteomics core as described previously (Dephoure et al., 2013). Briefly, protein

515 extracts were alkylated with iodoacetamide and digested with trypsin at a ratio of 1:50 (w/w)
516 trypsin to protein. Tryptic phosphopeptides were enriched by TiO_2-immobilized metal affinity
517 chromatography, washed with 70 % (v/v) EtOH and equilibrated in 1 % Nh4OH and three times
518 in 1M glycolic acid in 80 % (v/v) acetonitrile, 5% (v/v) trifluoroacetic acid. Peptides were eluted
519 and dried in a SpeedVac concentrator. Peptides were resuspended in 3 % (v/v) acetonitrile, 0.1 %
520 trifluoroacetic acid and twice in 0.1 % trifluoroacetic acid. Dried peptides were dissolved in LC-
521 MS/MS solvent (3 % acetonitrile and 0.1 % fluoroacetic acid prior to LC-MS/MS analysis using a
522 dual-pressure linear ion trap (Velos Pro) with a high-field Orbitrap mass analyzer as described
523 previously (Yue et al., 2015; Zhou et al., 2008).
524
525 **Phosphoproteomics analysis.** Data acquired on the Orbitrap were searched against a Uniprot
526 *Mus Musculus* protein database using TDPortal as previously described (Fornelli et al., 2017).
527 Annotations were extracted from UniProtKB, Gene Ontology (GO), and the Kyoto Encyclopedia
528 of Genes and Genomes (KEGG). Bioinformatics analyses including hierarchical clustering,
529 pathway analysis and annotation enrichment were performed with R v4.1.1 using the DEP
530 package (Zhang et al., 2018) for normalization and testing for significance. A varying number of
531 permutations of imputations and testing for significance were applied until the insulin receptor was
532 consistently found to be phosphorylated by insulin versus BSA. Pathway enrichment was
533 analyzed using the TopGO package using the classic Kolmogorov-Smirnov test. We applied
534 semantic similarity analysis between GO terms followed by principal coordinates analysis to
535 cluster and visualize enrichments. Unless otherwise stated, individual comparisons between
536 conditions across phosphopeptides was performed using empirical Bayes statistics followed by
537 adjustment for multiple testing with a p-value of * < 0.05, ** $p < 0.01$, *** $p < 0.001$ to be considered
538 significant. The minimum normalized intensity across the dataset was subtracted from each
539 normalized data point, and phosphorylation was calculated as a fraction of the maximum value of
540 all samples for each phosphopeptide. Plotted GO terms have P values <0.01 calculated using the

541 classic Kolmogorov-Smirnov test. The distribution diagram of shared and unique phosphosites
542 was obtained by retrieving the selected GO pathways for peptides detected in at least 1 sample
543 between treatments. Specific details on the significance of each test are described in the figure
544 legends.
545
546 **Immunohistochemistry and muscle fiber size quantification.** Tissues were snap-frozen and
547 cross-sectioned at 10 μm. For hematoxylin and eosin (H&E) staining, slides were stained with
548 hematoxylin for 3 min, washed with water and 95% ethanol, and stained with eosin for 30 min.
549 Sections were then washed with ethanol and xylene, and mounted with mounting medium. The
550 tissue slides were observed with a Nikon 80i upright light microscope using a 20 x objective lens.
551 Digital images were captured with a Nikon Digital Sight DS-Fi1 color camera and NIS-Elements
552 acquisition software. Muscle fiber sizes for the pectoralis, quadriceps, soleus, gastrocnemius, and
553 tibialis muscle tissues were determined by measuring cross-sectional area (μm2) using the Image
554 J (version 1.53e) software. The muscle fibers were manually outlined to obtain their measurement
555 data. Blind scoring by two independent investigators of the muscle tissues was done to unbiasedly
556 collect data for all categories of mice. The quantification of the average muscle fiber area was
557 performed on N = 3 independent muscle tissues from each genotype, with 2-4 photos taken from
558 each muscle tissue and average values calculated for each photo. Statistically significant
559 differences were determined using two-way ANOVA.
560
561 **Indirect calorimetry, food intake and physiological measurements.** Oxygen consumption
562 (VO_2), respiratory exchange ratio, movement, and food intake in eight-to-twelve-week-old WT and
563 Ism1-KO mice were measured using the environment-controlled home-cage CLAMS system
564 (Columbus Instruments, Columbus, OH, USA) at the Stanford Diabetes Research Center. Mice
565 were maintained on a chow diet and housed at 20-22°C in the cages for 24 h prior to the recording.
566 Energy expenditure calculations were not normalized for body weight. RER and locomotion were

567 analyzed using ANOVA. All other calorimetry measurements in mice were analyzed using
568 ANCOVA using the CalR version 1.3 without the remove outliers feature (Mina et al., 2018). The
569 muscle strength in the hindlimbs was measured with a grip meter. The mice were trained to
570 grasp a horizontal bar while being pulled by their tail. The force (expressed in Newton) was
571 recorded by a sensor.
572
573 **Single-cell RNA sequencing of skeletal muscle in mice.** Single-cell RNA sequencing data was
574 re-analyzed from a previously published dataset performed on single-cell suspension from murine
575 tibialis anterior skeletal muscles (Baht et al., 2020). Briefly, tibialis anterior muscles from three
576 injured mice were pooled as well as three uninjured mice to generate two samples used for
577 scRNA-Seq. Three thousand single cells from each of the two samples were barcoded and cDNA
578 generated using 10X Genomics Chromium Drop-seq platform and sequencing on Illumina 2500
579 platform. 10X Genomics Cell Ranger software was used to demultiplex and align reads. Seurat
580 (V4.2) package was used to perform quality control, sample normalization and clustering for cell
581 type identification. Downstream analyses included gene analysis of the genes of interests
582 associated with cell clusters.
583
584 **Expression and purification of recombinant proteins.** The Ism1 proteins were generated by
585 transient transfection of mouse Ism1 with C-terminal Myc-6X-his tag DNA plasmids Addgene
586 (#173046) into Expi293F cells. Recombinant proteins were produced in mammalian Expi293F
587 cells using large-scale transient DNA transfection and purified using Cobalt columns and buffer
588 exchanged to PBS. Protein purity and integrity were assessed with SDS page, Superdex200 size
589 exclusion column and endotoxin assay. Every protein batch produced was tested for bioactivity
590 by measuring the induction of $pAKT^{S473}$ signaling in 3T3-F442A cells as described previously
591 (Jiang et al., 2021). All proteins were aliquoted and stored at -80 °C and not used for more than
592 three freeze-thaws.

593

594 **Culture and differentiation of C2C12 cells.** C2C12 cells (#CRL-1772, ATCC) were cultured in
595 DMEM with 10 % FBS. Cells were passaged every two days and were not allowed to reach more
596 than 70 % confluency. For differentiation, media was replaced with DMEM with 2 % horse serum
597 and cultured for four days to induce myotube formation within 4-6 days as described
598 previously(Risson et al., 2009; Sandri et al., 2004).

599

600 ***In vivo* and *in vitro* protein synthesis.** *In vivo* protein synthesis was measured by incorporation
601 of [^{35}S]-methionine into proteins isolated from skeletal muscle in mice. Briefly, mice fasted for 1h
602 were I.P. injected with 2.5 μCi/gram [^{35}S]-methionine diluted in saline. Two hours after injection,
603 the quadriceps muscles were removed, weighed, and snap-frozen in liquid nitrogen. The tissues
604 were homogenized using a hand-held homogenizer in RIPA buffer containing protease inhibitor
605 cocktail (Roche) and centrifuged at 4 °C to remove cell debris. Protein concentration in the
606 supernatant was determined by BCA assay (Thermo Fischer Scientific, Waltham, MA, USA), and
607 total protein content was calculated by multiplying the protein concentration by the supernatant
608 volume. Proteins were extracted using TCA precipitation and the radioactivity was counted on a
609 scintillation counter. Protein synthesis in C2C12 cells was measured by incorporation of [^{35}S]-
610 methionine into proteins using a modified protocol developed for skeletal myotubes (Hong-Brown
611 et al., 2007; Kazi and Lang, 2010; Méchin et al., 2007) as described previously (Schmidt et al.,
612 2009). For [^{35}S]-methionine incorporation, C2C12 cells were treated with BSA, recombinant Ism1
613 or Igf1 with the addition of 0.5 μCi [^{35}S]-methionine (#NEG009L005MC, PerkinElmer, Waltham,
614 MA, USA) for 48h. For [^{35}S]-methionine incorporation in the presence or absence of inhibitors,
615 C2C12 cells were treated with DMSO or 100 nM Rapamycin for 2h, followed by treatments with
616 BSA, recombinant Ism1 or Igf1 for 1h. Subsequently, 0.5 μCi [^{35}S]-methionine (#NEG009L005MC,
617 PerkinElmer) was added for another 1h. To stop the incubation, cells were washed in ice-cold

618 PBS three times. Proteins were extracted using TCA precipitation and the radioactivity was
619 counted on a scintillation counter.
620
621 **Gene expression analysis.** Total RNA from cultured cells or tissues was isolated using TRIzol
622 (Thermo Fischer Scientific, Waltham, MA, USA) and Rneasy mini kits (QIAGEN, Hilden,
623 Germany). RNA was reverse transcribed using the ABI high-capacity cDNA synthesis kit. For q-
624 RT-pcr analysis, cDNA, primers and SYBR-green fluorescent dye (Bimake, Houston, TX, USA)
625 were used. Relative mRNA expression was determined by normalization to Cyclophilin levels
626 using the ΔΔCt method.
627
628 **Western blots and molecular analyses.** For western blotting, homogenized tissues or whole-
629 cell lysates, samples were lysed in RIPA buffer containing protease inhibitor cocktail (Roche,
630 Basel, Switzerland) and phosphatase inhibitor cocktail (Roche, Basel, Switzerland), prepared in
631 4X LDS Sample Buffer (Invitrogen, Waltham, MA, USA) and separated by SDS-PAGE and
632 transferred to Immobilon 0.45μm membranes (Millipore, Burlington, MA, USA). The antibodies
633 used are as follows: Rabbit monoclonal anti-p-AKT1/2 (Ser473) (#4060), AKT1 (pan) (#4691
634 CST), rabbit monoclonal anti-p-mTOR (Ser2448) (D9C2), rabbit polyclonal anti-p-S6
635 Ribosomal Protein (Ser235/236) (Cat#2211 CST), ribosomal protein S6 (#2217 CST) from Cell
636 Signaling. Mouse monoclonal anti-beta Actin AC-15 HRP (#AB49900) and OXPHOS rodent
637 antibody (#ab110413) were from Abcam. Donkey anti-rabbit IgG (HRP) (#NA934) and sheep
638 anti-mouse IgG (HRP) (#NA931) were from Cytiva (GE). Recombinant Igf1 (#791-MG-050) was
639 from R&D systems. The mammalian expression plasmid for Ism1 with C-terminal myc-6xhis tag
640 plasmid for recombinant Ism1 protein production was from Addgene (#173046).
641
642 **Statistical analyses.** Values for *N* represent biological replicates for cultured cell experiments or
643 individual animals for *in vivo* experiments. Group-housed mice within eight weeks of age were

644 used for comparative studies. Mice were randomly assigned to treatment groups for *in vivo*
645 studies. Significant differences between the two groups (* $p < 0.05$, ** $p < 0.01$, *** $p < 0.001$)
646 were evaluated using a two-tailed, unpaired Student´s t-test as the sample groups displayed a
647 normal distribution and comparable variance (Prism9 software; GraphPad). Two-way ANOVA
648 with repeated measures was used for body weight and repeated measurements (* $p < 0.05$, ** p
649 <0.01, *** $p < 0.001$). All data are presented as the standard error of mean (S.E.M.) or as
650 described in the figure legend. Specific details for *N* values are noted in each figure legend.
651

652 ## Acknowledgements

653 K.J.S. was supported by NIH grants DK125260, DK111916, the Stanford Diabetes Research
654 Center P30DK116074, the Jacob Churg Foundation, the McCormick and Gabilan Award, the
655 Weintz Family COVID-19 research fund, American Heart Association (AHA), the Stanford School
656 of Medicine, and the Stanford Cardiovascular Institute (CVI). M.Z. was supported by the American
657 Heart Association (AHA) postdoctoral fellowship (905674). L.V. was supported by Stanford
658 School of Medicine Dean's Postdoctoral Fellowship. E.B.M. was supported by Stanford School of
659 Medicine Dean's Postdoctoral Fellowship and the American Heart Association (AHA) postdoctoral
660 fellowship (18POST34030448). D.E.L. was supported by NIH training grant T32HL007057.
661 J.P.W. was supported by NIH/NIA grant K01AG056664 and R21AG065943 and Borden Scholar
662 Award through Duke University. N.C. was supported by the American Heart Association (AHA)
663 SURE award (882082). N.B.D.S. was supported by the Carlsberg Foundation Internationalization
664 Fellowship. C.V.R. was supported by the Weintz family COVID-19 research fund, the Stanford
665 Women's Cancer Center and the Stanford Cancer Institute, The Jacob Churg award, and the
666 Children's Cancer Research Foundation. We thank the Stanford University Pathology Histology
667 core facility, and the Pathology Department for microscopy equipment. We thank the Proteomics
668 core at Northwestern University for assistance with the phosphoproteomic analysis, and Pratima

669 Nallagatla at Stanford University for assistance with the data processing. This work was supported
670 by the Stanford Diabetes Research Center (NIH grant #P30DK116074). Some illustrations were
671 created with Biorender under a paid subscription.
672

673 ## Additional information

674 **Competing interests**

675 The authors declare that no competing interests exist.

676

677 **Author Contributions**

678 Conceptualization, M.Z, and K.J.S.; Methodology, M.Z, N.B.D.S., K.J.S. Investigation, M.Z.,
679 N.B.D.S., L.V., L.U., E.B.M., D.E.L., J.P.W., N.C., Q.N., C.V.R., K.J.S., Writing - Original Draft,
680 M.Z, N.B.D.S., K.J.S.; Writing - Review & Editing, M.Z, N.B.D.S., L.V., K.J.S.; Resources, C.V.R.,
681 K.J.S.; Supervision and funding acquisition, K.J.S.

682

683 ## Additional files

684

685 **Source data 1**

686 Unedited raw western blot images in Figure 1, 3, 5 and 6.

687

688 **Figure 1—supplement 1**

689 Quality controls for the phosphoproteomics analysis.
690 (A) Total phosphosites identified in cells treated with 100 nM bovine serum albumin (BSA), 100
691 nM Ism1, or 100 nM insulin for 5 minutes.

692

693 **Figure 1—source data 1**

694 List of phosphosites significantly different between treatments for Figure 1E.

695

696 **Figure 1—source data 2**

697 List of shared and unique phosphosites between treatments for selected GO pathways for Figure

698 1F.

699

700 **Figure 1—source data 3**

701 Uncropped western blot images with relevant bands labelled.

702

703 **Figure 2—supplement 1**

704 Insulin receptor substrate-1 and 2 (Irs1/2) phosphorylation status in response to Ism1 or insulin.

705 (A) Heatmap of differentially phosphorylated Irs1 and Irs2 phosphosites by Ism1 relative to

706 insulin (n = 2, individual comparisons between conditions across phosphopeptides using

707 empirical Bayes statistics followed by adjustment for multiple testing using false discovery rate,

708 *$p < 0.05$, **$p < 0.01$, ***$p < 0.001$).

709

710 **Figure 2—source data 1**

711 Enriched pathways for proteins with phosphosites significantly different between Ism1 and BSA

712 clustered by semantic similarity.

713

714 **Figure 2—source data 2**

715 Raw data related to Figure 2B, and E-N.

716

717 **Figure 3—supplement 1**

718 Ism1 acts non-cell autonomously on muscle cells.

719 (A) UMAP plot of single-cell RNA sequencing of isolated cells from mouse skeletal muscle. (B)

720 Expression of *Pdgfra* in fibro-adipose precursors within the muscle. (C) Low expression of *Ism1*
721 within the muscle tissue. (D) Low expression of Ism1 in myocytes and myoblasts.
722
723 **Figure 3—supplement 2**
724 Ism1 ablation does not reduce muscle mass or muscle fiber size in all tissue locations.
725 (A-B) Quantification of average muscle fiber area in gastrocnemius (A) and tibialis (B) in a blinded
726 fashion by two independent investigators (WT fed, n = 3; Ism1-KO fed, n = 3, WT fasted, n = 3;
727 Ism1-KO fasted, n = 3, two-way ANOVA, *p < 0.05, **p < 0.01, ***p < 0.001). (C) Heart mass of
728 WT and Ism1-KO mice in the fed or fasted groups (WT fed, n = 3; Ism1-KO fed, n = 3; WT fasted,
729 n = 3; Ism1-KO fasted, n = 3, two-way ANOVA). (D-F) Muscle masses of gastrocnemius (D),
730 tibialis (E), and quadriceps (F) of WT and Ism1-KO mice in the fed or fasted groups (WT fed, n =
731 3; Ism1-KO fed, n = 3; WT fasted, n = 3; Ism1-KO fasted, n = 3, two-way ANOVA). Bar graphs
732 show mean ± SEM.
733
734 **Figure 3—source data 1**
735 Raw data related to Figure 3B, D, and E.
736
737 **Figure 3—source data 2**
738 Uncropped western blot images with relevant bands labelled.
739
740 **Figure 4—source data 1**
741 Raw data related to Figure 4B, C, and E-G.
742
743 **Figure 5—source data 1**
744 Raw data related to Figure 5A-D and F-H.
745

Figure 5—source data 2

Uncropped western blot images with relevant bands labelled.

Figure 6—source data 1

Raw data related to Figure 6A and C-G.

Figure 6—source data 2

Uncropped western blot images with relevant bands labelled.

Data availability

All data generated or analyzed during this study are included in the manuscript and supporting files. The phosphoproteomics dataset has been deposited to ProteomeXchange Consortium through JPost PXD031719 (JPST001484)(Okuda et al., 2017). The code for all analysis related to phosphoproteomic data is available at https://github.com/Svensson-Lab/Isthmin-1/tree/F442A_phosphoproteomics. The single-cell RNA sequencing data was re-analyzed from a previously published dataset (Baht et al., 2020). All generated reagents will be shared upon request, including Ism1 recombinant proteins and Ism1-KO and Ism1-flox mice. Further information and requests for resources and reagents should be directed to and will be fulfilled by the Lead Contact, Dr. Katrin J. Svensson (katrinjs@stanford.edu).

References

Andersen, H., Nielsen, S., Mogensen, C.E., Jakobsen, J., 2004. Muscle strength in type 2 diabetes. Diabetes 53, 1543–1548. https://doi.org/10.2337/diabetes.53.6.1543

Baht, G.S., Bareja, A., Lee, D.E., Rao, R.R., Huang, R., Huebner, J.L., Bartlett, D.B., Hart, C.R., Gibson, J.R., Lanza, I.R., Kraus, V.B., Gregory, S.G., Spiegelman, B.M., White, J.P., 2020. Meteorin-like facilitates skeletal muscle repair through a Stat3/IGF-1 mechanism. Nature metabolism 2, 278–289. https://doi.org/10.1038/s42255-020-0184-y

Bhardwaj, G., Penniman, C.M., Jena, J., Suarez Beltran, P.A., Foster, C., Poro, K., Junck, T.L., Hinton, A.O.J., Souvenir, R., Fuqua, J.D., Morales, P.E., Bravo-Sagua, R., Sivitz, W.I., Lira, V.A., Abel, E.D., O'Neill, B.T., 2021. Insulin and IGF-1 receptors regulate complex I-dependent mitochondrial bioenergetics and supercomplexes via FoxOs in muscle. The Journal of clinical investigation 131. https://doi.org/10.1172/JCI146415

Bodine, S.C., Baehr, L.M., 2014. Skeletal muscle atrophy and the E3 ubiquitin ligases MuRF1 and MAFbx/atrogin-1. American journal of physiology. Endocrinology and metabolism 307, E469–E484. https://doi.org/10.1152/ajpendo.00204.2014

Bodine, S.C., Stitt, T.N., Gonzalez, M., Kline, W.O., Stover, G.L., Bauerlein, R., Zlotchenko, E., Scrimgeour, A., Lawrence, J.C., Glass, D.J., Yancopoulos, G.D., 2001. Akt/mTOR pathway is a crucial regulator of skeletal muscle hypertrophy and can prevent muscle atrophy in vivo. Nature cell biology 3, 1014–1019. https://doi.org/10.1038/ncb1101-1014

Chauvin, C., Koka, V., Nouschi, A., Mieulet, V., Hoareau-Aveilla, C., Dreazen, A., Cagnard, N., Carpentier, W., Kiss, T., Meyuhas, O., Pende, M., 2014. Ribosomal protein S6 kinase activity controls the ribosome biogenesis transcriptional program. Oncogene 33, 474–483. https://doi.org/10.1038/onc.2012.606

Chen, P.-Y., Friesel, R., 2009. FGFR1 forms an FRS2-dependent complex with mTOR to regulate smooth muscle marker gene expression. Biochemical and biophysical research

796 communications 382, 424–429. https://doi.org/10.1016/j.bbrc.2009.03.040
797 Cohen, S., Nathan, J.A., Goldberg, A.L., 2015. Muscle wasting in disease: molecular
798 mechanisms and promising therapies. Nature reviews. Drug discovery 14, 58–74.
799 https://doi.org/10.1038/nrd4467
800 Dephoure, N., Gould, K.L., Gygi, S.P., Kellogg, D.R., 2013. Mapping and analysis of
801 phosphorylation sites: a quick guide for cell biologists. Molecular biology of the cell 24,
802 535–542. https://doi.org/10.1091/mbc.E12-09-0677
803 Deshmukh, A.S., 2016. Insulin-stimulated glucose uptake in healthy and insulin-resistant
804 skeletal muscle. Hormone Molecular Biology and Clinical Investigation 26, 13–24.
805 https://doi.org/10.1515/hmbci-2015-0041
806 Edinger, A.L., Thompson, C.B., 2002. Akt maintains cell size and survival by increasing mTOR-
807 dependent nutrient uptake. Molecular biology of the cell 13, 2276–2288.
808 https://doi.org/10.1091/mbc.01-12-0584
809 Fornelli, L., Durbin, K.R., Fellers, R.T., Early, B.P., Greer, J.B., LeDuc, R.D., Compton, P.D.,
810 Kelleher, N.L., 2017. Advancing Top-down Analysis of the Human Proteome Using a
811 Benchtop Quadrupole-Orbitrap Mass Spectrometer. Journal of proteome research 16,
812 609–618. https://doi.org/10.1021/acs.jproteome.6b00698
813 Glass, D.J., 2011. PI3 Kinase Regulation of Skeletal Muscle Hypertrophy and Atrophy, in:
814 Rommel, C., Vanhaesebroeck, B., Vogt, P.K. (Eds.), Phosphoinositide 3-Kinase in Health
815 and Disease: Volume 1. Springer Berlin Heidelberg, Berlin, Heidelberg, pp. 267–278.
816 https://doi.org/10.1007/82_2010_78
817 Gomes, M.D., Lecker, S.H., Jagoe, R.T., Navon, A., Goldberg, A.L., 2001. Atrogin-1, a muscle-
818 specific F-box protein highly expressed during muscle atrophy. Proceedings of the National
819 Academy of Sciences of the United States of America 98, 14440–14445.
820 https://doi.org/10.1073/pnas.251541198
821 Hawke, T.J., Garry, D.J., 2001. Myogenic satellite cells: physiology to molecular biology. Journal

822 of applied physiology (Bethesda, Md. : 1985) 91, 534–551.
823 https://doi.org/10.1152/jappl.2001.91.2.534
824 Hong-Brown, L.Q., Brown, C.R., Huber, D.S., Lang, C.H., 2007. Alcohol regulates eukaryotic
825 elongation factor 2 phosphorylation via an AMP-activated protein kinase-dependent
826 mechanism in C2C12 skeletal myocytes. The Journal of biological chemistry 282, 3702–
827 3712. https://doi.org/10.1074/jbc.M606593200
828 Huang, J., Manning, B.D., 2008. The TSC1-TSC2 complex: a molecular switchboard controlling
829 cell growth. The Biochemical journal 412, 179–190. https://doi.org/10.1042/BJ20080281
830 Humphrey, S.J., James, D.E., Mann, M., 2015. Protein Phosphorylation: A Major Switch
831 Mechanism for Metabolic Regulation. Trends in endocrinology and metabolism: TEM 26,
832 676–687. https://doi.org/10.1016/j.tem.2015.09.013
833 Humphrey, S.J., Yang, G., Yang, P., Fazakerley, D.J., Stöckli, J., Yang, J.Y., James, D.E.,
834 2013. Dynamic adipocyte phosphoproteome reveals that Akt directly regulates mTORC2.
835 Cell metabolism 17, 1009–1020. https://doi.org/10.1016/j.cmet.2013.04.010
836 Inoki, K., Li, Y., Xu, T., Guan, K.-L., 2003. Rheb GTPase is a direct target of TSC2 GAP activity
837 and regulates mTOR signaling. Genes & development 17, 1829–1834.
838 https://doi.org/10.1101/gad.1110003
839 Jackman, R.W., Kandarian, S.C., 2004. The molecular basis of skeletal muscle atrophy.
840 American journal of physiology. Cell physiology 287, C834-43.
841 https://doi.org/10.1152/ajpcell.00579.2003
842 Jaiswal, N., Gavin, M., Loro, E., Sostre-Colón, J., Roberson, P.A., Uehara, K., Rivera-Fuentes,
843 N., Neinast, M., Arany, Z., Kimball, S.R., Khurana, T.S., Titchenell, P.M., 2022. AKT
844 controls protein synthesis and oxidative metabolism via combined mTORC1 and FOXO1
845 signalling to govern muscle physiology. Journal of cachexia, sarcopenia and muscle 13,
846 495–514. https://doi.org/10.1002/jcsm.12846
847 Jaiswal, N., Gavin, M.G., Quinn 3rd, W.J., Luongo, T.S., Gelfer, R.G., Baur, J.A., Titchenell,

848 P.M., 2019. The role of skeletal muscle Akt in the regulation of muscle mass and glucose
849 homeostasis. Molecular metabolism 28, 1–13.
850 https://doi.org/10.1016/j.molmet.2019.08.001
851 Janssen, I., Heymsfield, S.B., Wang, Z.M., Ross, R., 2000. Skeletal muscle mass and
852 distribution in 468 men and women aged 18-88 yr. Journal of applied physiology
853 (Bethesda, Md. : 1985) 89, 81–88. https://doi.org/10.1152/jappl.2000.89.1.81
854 Jiang, Z., Zhao, M., Voilquin, L., Jung, Y., Aikio, M.A., Sahai, T., Dou, F.Y., Roche, A.M.,
855 Carcamo-Orive, I., Knowles, J.W., Wabitsch, M., Appel, E.A., Maikawa, C.L., Camporez,
856 J.P., Shulman, G.I., Tsai, L., Rosen, E.D., Gardner, C.D., Spiegelman, B.M., Svensson,
857 K.J., 2021. Isthmin-1 is an adipokine that promotes glucose uptake and improves glucose
858 tolerance and hepatic steatosis. Cell metabolism.
859 https://doi.org/10.1016/j.cmet.2021.07.010
860 Kazi, A.A., Lang, C.H., 2010. PRAS40 regulates protein synthesis and cell cycle in C2C12
861 myoblasts. Molecular medicine (Cambridge, Mass.) 16, 359–371.
862 https://doi.org/10.2119/molmed.2009.00168
863 Lai, K.-M. V, Gonzalez, M., Poueymirou, W.T., Kline, W.O., Na, E., Zlotchenko, E., Stitt, T.N.,
864 Economides, A.N., Yancopoulos, G.D., Glass, D.J., 2004. Conditional activation of akt in
865 adult skeletal muscle induces rapid hypertrophy. Molecular and cellular biology 24, 9295–
866 9304. https://doi.org/10.1128/MCB.24.21.9295-9304.2004
867 Lam, T.Y.W., Nguyen, N., Peh, H.Y., Shanmugasundaram, M., Chandna, R., Tee, J.H., Ong,
868 C.B., Hossain, M.Z., Venugopal, S., Zhang, T., Xu, S., Qiu, T., Kong, W.T., Chakarov, S.,
869 Srivastava, S., Liao, W., Kim, J.-S., Teh, M., Ginhoux, F., Fred Wong, W.S., Ge, R., 2022.
870 ISM1 protects lung homeostasis via cell-surface GRP78-mediated alveolar macrophage
871 apoptosis. Proceedings of the National Academy of Sciences of the United States of
872 America 119. https://doi.org/10.1073/pnas.2019161119
873 Laurens, C., Grundler, F., Damiot, A., Chery, I., Le Maho, A.-L., Zahariev, A., Le Maho, Y.,

874 Bergouignan, A., Gauquelin-Koch, G., Simon, C., Blanc, S., Wilhelmi de Toledo, F., 2021.
875 Is muscle and protein loss relevant in long-term fasting in healthy men? A prospective trial
876 on physiological adaptations. Journal of cachexia, sarcopenia and muscle 12, 1690–1703.
877 https://doi.org/10.1002/jcsm.12766
878 Lecker, S.H., Solomon, V., Mitch, W.E., Goldberg, A.L., 1999. Muscle protein breakdown and
879 the critical role of the ubiquitin-proteasome pathway in normal and disease states. The
880 Journal of nutrition 129, 227S-237S. https://doi.org/10.1093/jn/129.1.227S
881 Li, C., Zhong, S., Ni, S., Liu, Z., Zhang, S., Ji, G., 2021. Zebrafish Ism1 is a novel antiviral factor
882 that positively regulates antiviral immune responses. Developmental and comparative
883 immunology 125, 104210. https://doi.org/10.1016/j.dci.2021.104210
884 Lin, J., Wu, H., Tarr, P.T., Zhang, C.-Y., Wu, Z., Boss, O., Michael, L.F., Puigserver, P., Isotani,
885 E., Olson, E.N., Lowell, B.B., Bassel-Duby, R., Spiegelman, B.M., 2002. Transcriptional co-
886 activator PGC-1 alpha drives the formation of slow-twitch muscle fibres. Nature 418, 797–
887 801. https://doi.org/10.1038/nature00904
888 Luo, J., Manning, B.D., Cantley, L.C., 2003. Targeting the PI3K-Akt pathway in human cancer:
889 Rationale and promise. Cancer Cell 4, 257–262. https://doi.org/10.1016/S1535-
890 6108(03)00248-4
891 Ma, S., Dong, Z., Huang, Y., Liu, J.-Y., Zhang, J.-T., 2022. eIF3a regulation of mTOR signaling
892 and translational control via HuR in cellular response to DNA damage. Oncogene 41,
893 2431–2443. https://doi.org/10.1038/s41388-022-02262-5
894 Mammucari, C., Milan, G., Romanello, V., Masiero, E., Rudolf, R., Del Piccolo, P., Burden, S.J.,
895 Di Lisi, R., Sandri, C., Zhao, J., Goldberg, A.L., Schiaffino, S., Sandri, M., 2007. FoxO3
896 controls autophagy in skeletal muscle in vivo. Cell metabolism 6, 458–471.
897 https://doi.org/10.1016/j.cmet.2007.11.001
898 Méchin, V., Damerval, C., Zivy, M., 2007. Total protein extraction with TCA-acetone. Methods in
899 molecular biology (Clifton, N.J.) 355, 1–8. https://doi.org/10.1385/1-59745-227-0:1

900 Mina, A.I., LeClair, R.A., LeClair, K.B., Cohen, D.E., Lantier, L., Banks, A.S., 2018. CalR: A
901 Web-Based Analysis Tool for Indirect Calorimetry Experiments. Cell Metabolism 28, 656-
902 666.e1. https://doi.org/https://doi.org/10.1016/j.cmet.2018.06.019
903 Minard, A.Y., Tan, S.X., Yang, P., Fazakerley, D.J., Domanova, W., Parker, B.L., Humphrey,
904 S.J., Jothi, R., Stöckli, J., James, D.E., 2016. mTORC1 Is a Major Regulatory Node in the
905 FGF21 Signaling Network in Adipocytes. Cell Reports 17, 29–36.
906 https://doi.org/10.1016/j.celrep.2016.08.086
907 Moro, T., Ebert, S.M., Adams, C.M., Rasmussen, B.B., 2016. Amino Acid Sensing in Skeletal
908 Muscle. Trends in endocrinology and metabolism: TEM 27, 796–806.
909 https://doi.org/10.1016/j.tem.2016.06.010
910 Musarò, A., McCullagh, K.J., Naya, F.J., Olson, E.N., Rosenthal, N., 1999. IGF-1 induces
911 skeletal myocyte hypertrophy through calcineurin in association with GATA-2 and NF-
912 ATc1. Nature 400, 581–585. https://doi.org/10.1038/23060
913 Nishizawa, S., Koya, T., Ohno, Y., Goto, A., Ikuita, A., Suzuki, M., Ohira, T., Egawa, T., Nakai,
914 A., Sugiura, T., Ohira, Y., Yoshioka, T., Beppu, M., Goto, K., 2013. Regeneration of injured
915 skeletal muscle in heat shock transcription factor 1-null mice. Physiological reports 1,
916 e00071. https://doi.org/10.1002/phy2.71
917 Okuda, S., Watanabe, Y., Moriya, Y., Kawano, S., Yamamoto, T., Matsumoto, M., Takami, T.,
918 Kobayashi, D., Araki, N., Yoshizawa, A.C., Tabata, T., Sugiyama, N., Goto, S., Ishihama,
919 Y., 2017. jPOSTrepo: an international standard data repository for proteomes. Nucleic
920 acids research 45, D1107–D1111. https://doi.org/10.1093/nar/gkw1080
921 Osório, L., Wu, X., Zhou, Z., 2014. Distinct spatiotemporal expression of ISM1 during mouse
922 and chick development. Cell Cycle 13, 1571–1582. https://doi.org/10.4161/cc.28494
923 Pallafacchina, G., Calabria, E., Serrano, A.L., Kalhovde, J.M., Schiaffino, S., 2002. A protein
924 kinase B-dependent and rapamycin-sensitive pathway controls skeletal muscle growth but
925 not fiber type specification. Proceedings of the National Academy of Sciences 99, 9213 LP

926 – 9218. https://doi.org/10.1073/pnas.142166599
927 Park, S.W., Goodpaster, B.H., Strotmeyer, E.S., Kuller, L.H., Broudeau, R., Kammerer, C., de
928 Rekeneire, N., Harris, T.B., Schwartz, A. V, Tylavsky, F.A., Cho, Y., Newman, A.B., 2007.
929 Accelerated loss of skeletal muscle strength in older adults with type 2 diabetes: the
930 health, aging, and body composition study. Diabetes care 30, 1507–1512.
931 https://doi.org/10.2337/dc06-2537
932 Pera, E.M., Kim, J.I., Martinez, S.L., Brechner, M., Li, S.Y., Wessely, O., De Robertis, E.M.,
933 2002. Isthmin is a novel secreted protein expressed as part of the Fgf-8 synexpression
934 group in the Xenopus midbrain-hindbrain organizer. Mechanisms of Development 116,
935 169–172. https://doi.org/10.1016/S0925-4773(02)00123-5
936 Perry, B.D., Caldow, M.K., Brennan-Speranza, T.C., Sbaraglia, M., Jerums, G., Garnham, A.,
937 Wong, C., Levinger, P., Asrar Ul Haq, M., Hare, D.L., Price, S.R., Levinger, I., 2016.
938 Muscle atrophy in patients with Type 2 Diabetes Mellitus: roles of inflammatory pathways,
939 physical activity and exercise. Exercise immunology review 22, 94–109.
940 Peterson, M.D., Zhang, P., Choksi, P., Markides, K.S., Al Snih, S., 2016. Muscle Weakness
941 Thresholds for Prediction of Diabetes in Adults. Sports medicine (Auckland, N.Z.) 46, 619–
942 628. https://doi.org/10.1007/s40279-015-0463-z
943 Powers, E.T., Morimoto, R.I., Dillin, A., Kelly, J.W., Balch, W.E., 2009. Biological and chemical
944 approaches to diseases of proteostasis deficiency. Annual review of biochemistry 78, 959–
945 991. https://doi.org/10.1146/annurev.biochem.052308.114844
946 Risson, V., Mazelin, L., Roceri, M., Sanchez, H., Moncollin, V., Corneloup, C., Richard-Bulteau,
947 H., Vignaud, A., Baas, D., Defour, A., Freyssenet, D., Tanti, J.-F., Le-Marchand-Brustel, Y.,
948 Ferrier, B., Conjard-Duplany, A., Romanino, K., Bauché, S., Hantaï, D., Mueller, M.,
949 Kozma, S.C., Thomas, G., Rüegg, M.A., Ferry, A., Pende, M., Bigard, X., Koulmann, N.,
950 Schaeffer, L., Gangloff, Y.-G., 2009. Muscle inactivation of mTOR causes metabolic and
951 dystrophin defects leading to severe myopathy. The Journal of cell biology 187, 859–874.

952 https://doi.org/10.1083/jcb.200903131
953 Rodgers, J.T., Schroeder, M.D., Ma, C., Rando, T.A., 2017. HGFA Is an Injury-Regulated
954 Systemic Factor that Induces the Transition of Stem Cells into G(Alert). Cell reports 19,
955 479–486. https://doi.org/10.1016/j.celrep.2017.03.066
956 Roubenoff, R., Castaneda, C., 2001. Sarcopenia-understanding the dynamics of aging muscle.
957 JAMA. https://doi.org/10.1001/jama.286.10.1230
958 Ruiz-Ojeda, F.J., Anguita-Ruiz, A., Rico, M.C., Leis, R., Bueno, G., Gil-Campos, M., Gil, Á.,
959 Aguilera, C.M., 2022. Serum levels of the novel adipokine isthmin-1 are associated with
960 obesity in pubertal boys. medRxiv 2022.03.02.22271664.
961 https://doi.org/10.1101/2022.03.02.22271664
962 Sandri, M., Sandri, C., Gilbert, A., Skurk, C., Calabria, E., Picard, A., Walsh, K., Schiaffino, S.,
963 Lecker, S.H., Goldberg, A.L., 2004. Foxo transcription factors induce the atrophy-related
964 ubiquitin ligase atrogin-1 and cause skeletal muscle atrophy. Cell 117, 399–412.
965 https://doi.org/10.1016/s0092-8674(04)00400-3
966 Scanga, S.E., Ruel, L., Binari, R.C., Snow, B., Stambolic, V., Bouchard, D., Peters, M., Calvieri,
967 B., Mak, T.W., Woodgett, J.R., Manoukian, A.S., 2000. The conserved PI3'K/PTEN/Akt
968 signaling pathway regulates both cell size and survival in Drosophila. Oncogene 19, 3971–
969 3977. https://doi.org/10.1038/sj.onc.1203739
970 Schmidt, E.K., Clavarino, G., Ceppi, M., Pierre, P., 2009. SUnSET, a nonradioactive method to
971 monitor protein synthesis. Nature methods 6, 275–277. https://doi.org/10.1038/nmeth.1314
972 Shulman, G.I., Rothman, D.L., Jue, T., Stein, P., DeFronzo, R.A., Shulman, R.G., 1990.
973 Quantitation of muscle glycogen synthesis in normal subjects and subjects with non-
974 insulin-dependent diabetes by 13C nuclear magnetic resonance spectroscopy. The New
975 England journal of medicine 322, 223–228.
976 https://doi.org/10.1056/NEJM199001253220403
977 Uhlén, M., Karlsson, M.J., Hober, A., Svensson, A.-S., Scheffel, J., Kotol, D., Zhong, W.,

978 Tebani, A., Strandberg, L., Edfors, F., Sjöstedt, E., Mulder, J., Mardinoglu, A., Berling, A.,
979 Ekblad, S., Dannemeyer, M., Kanje, S., Rockberg, J., Lundqvist, M., Malm, M., Volk, A.-L.,
980 Nilsson, P., Månberg, A., Dodig-Crnkovic, T., Pin, E., Zwahlen, M., Oksvold, P., von
981 Feilitzen, K., Häussler, R.S., Hong, M.-G., Lindskog, C., Ponten, F., Katona, B., Vuu, J.,
982 Lindström, E., Nielsen, J., Robinson, J., Ayoglu, B., Mahdessian, D., Sullivan, D., Thul, P.,
983 Danielsson, F., Stadler, C., Lundberg, E., Bergström, G., Gummesson, A., Voldborg, B.G.,
984 Tegel, H., Hober, S., Forsström, B., Schwenk, J.M., Fagerberg, L., Sivertsson, Å., 2019.
985 The human secretome. Science signaling 12. https://doi.org/10.1126/scisignal.aaz0274
986 Um, S.H., Frigerio, F., Watanabe, M., Picard, F., Joaquin, M., Sticker, M., Fumagalli, S.,
987 Allegrini, P.R., Kozma, S.C., Auwerx, J., Thomas, G., 2004. Absence of S6K1 protects
988 against age- and diet-induced obesity while enhancing insulin sensitivity. Nature 431, 200–
989 205. https://doi.org/10.1038/nature02866
990 Valle-Rios, R., Maravillas-Montero, J.L., Burkhardt, A.M., Martinez, C., Buhren, B.A., Homey, B.,
991 Gerber, P.A., Robinson, O., Hevezi, P., Zlotnik, A., 2014. Isthmin 1 is a secreted protein
992 expressed in skin, mucosal tissues, and NK, NKT, and Th17 cells. Journal of Interferon and
993 Cytokine Research 34, 795–801. https://doi.org/10.1089/jir.2013.0137
994 Velloso, C.P., 2008. Regulation of muscle mass by growth hormone and IGF-I. British journal of
995 pharmacology 154, 557–568. https://doi.org/10.1038/bjp.2008.153
996 Watt, K.I., Turner, B.J., Hagg, A., Zhang, X., Davey, J.R., Qian, H., Beyer, C., Winbanks, C.E.,
997 Harvey, K.F., Gregorevic, P., 2015. The Hippo pathway effector YAP is a critical regulator
998 of skeletal muscle fibre size. Nature communications 6, 6048.
999 https://doi.org/10.1038/ncomms7048
1000 Wilson, E.M., Rotwein, P., 2007. Selective control of skeletal muscle differentiation by Akt1. The
1001 Journal of biological chemistry 282, 5106–5110. https://doi.org/10.1074/jbc.C600315200
1002 Wu, Y., Liang, X., Ni, J., Zhao, R., Shao, S., Lu, S., Han, W., Yu, L., 2021. Effect of ISM1 on the
1003 Immune Microenvironment and Epithelial-Mesenchymal Transition in Colorectal Cancer.

1004 Frontiers in cell and developmental biology 9, 681240.
1005 https://doi.org/10.3389/fcell.2021.681240
1006 Wu, Z., Puigserver, P., Andersson, U., Zhang, C., Adelmant, G., Mootha, V., Troy, A., Cinti, S.,
1007 Lowell, B., Scarpulla, R.C., Spiegelman, B.M., 1999. Mechanisms controlling mitochondrial
1008 biogenesis and respiration through the thermogenic coactivator PGC-1. Cell 98, 115–124.
1009 https://doi.org/10.1016/S0092-8674(00)80611-X
1010 Yenush, L., White, M.F., 1997. The IRS-signalling system during insulin and cytokine action.
1011 BioEssays : news and reviews in molecular, cellular and developmental biology 19, 491–
1012 500. https://doi.org/10.1002/bies.950190608
1013 Yue, X., Schunter, A., Hummon, A.B., 2015. Comparing multistep immobilized metal affinity
1014 chromatography and multistep TiO2 methods for phosphopeptide enrichment. Analytical
1015 chemistry 87, 8837–8844. https://doi.org/10.1021/acs.analchem.5b01833
1016 Zhang, X., Smits, A.H., van Tilburg, G.B., Ovaa, H., Huber, W., Vermeulen, M., 2018.
1017 Proteome-wide identification of ubiquitin interactions using UbIA-MS. Nature protocols 13,
1018 530–550. https://doi.org/10.1038/nprot.2017.147
1019 Zhao, M., Jung, Y., Jiang, Z., Svensson, K.J., 2020. Regulation of Energy Metabolism by
1020 Receptor Tyrosine Kinase Ligands. Frontiers in Physiology.
1021 https://doi.org/10.3389/fphys.2020.00354
1022 Zhou, H., Ye, M., Dong, J., Han, G., Jiang, X., Wu, R., Zou, H., 2008. Specific phosphopeptide
1023 enrichment with immobilized titanium ion affinity chromatography adsorbent for
1024 phosphoproteome analysis. Journal of proteome research 7, 3957–3967.
1025 https://doi.org/10.1021/pr800223m
1026 Zhou, W., Feng, X., Wu, Y., Benge, J., Zhang, Z., Chen, Z., 2009. FGF-receptor substrate 2
1027 functions as a molecular sensor integrating external regulatory signals into the FGF
1028 pathway. Cell research 19, 1165–1177. https://doi.org/10.1038/cr.2009.95
1029

1030

1031

1032

Figure 1—supplement 1

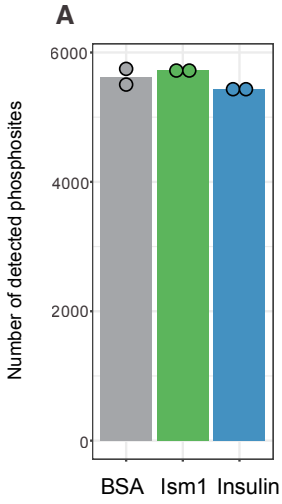

Figure 2—supplement 1

A

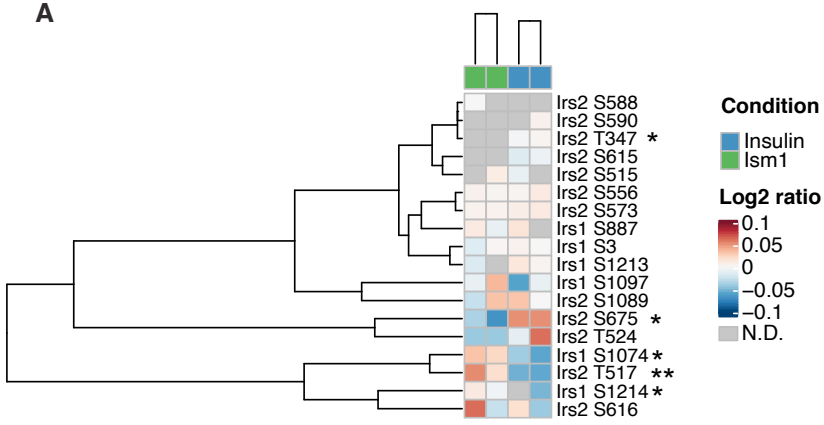

Figure 3—supplement 1

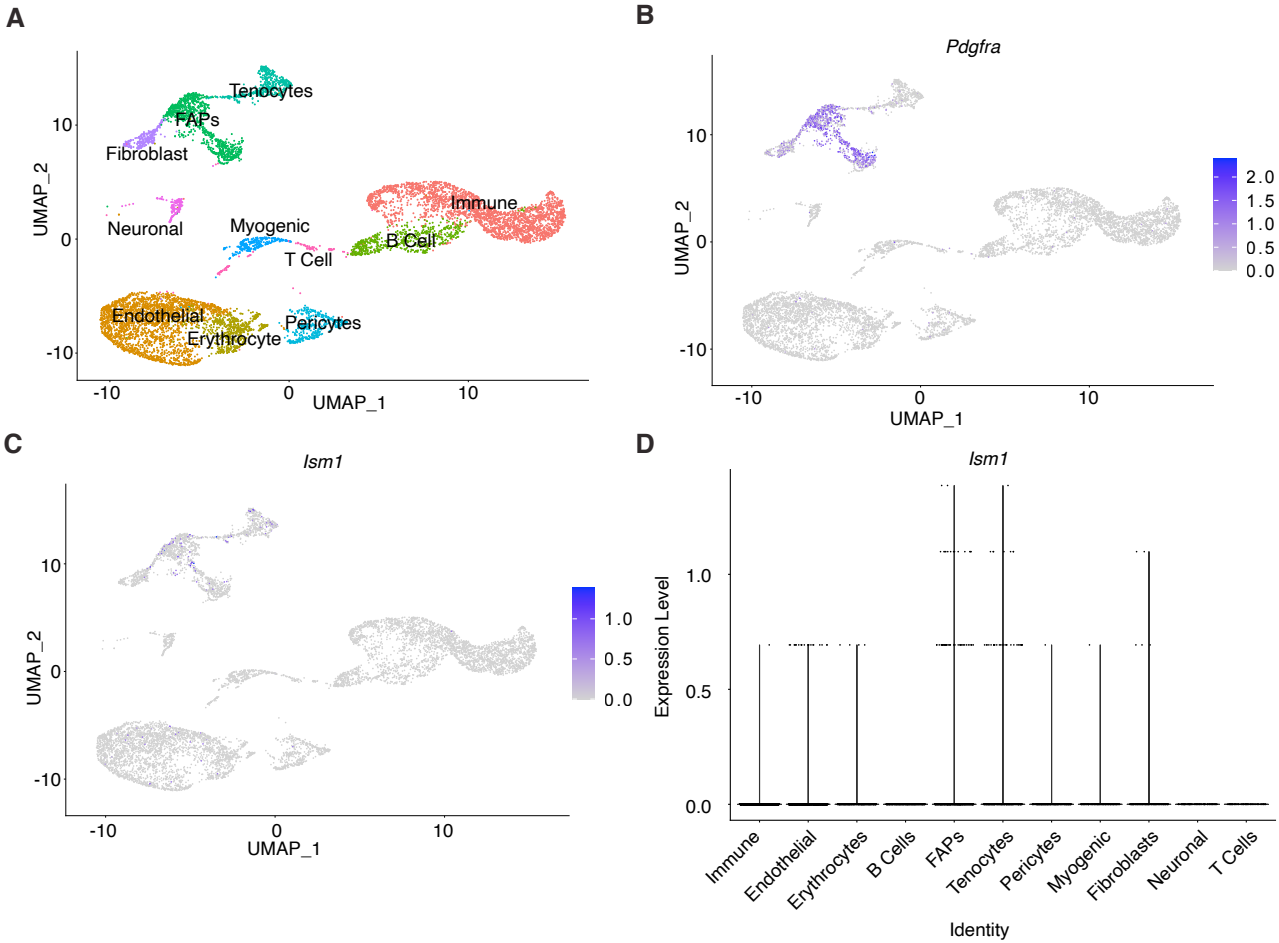
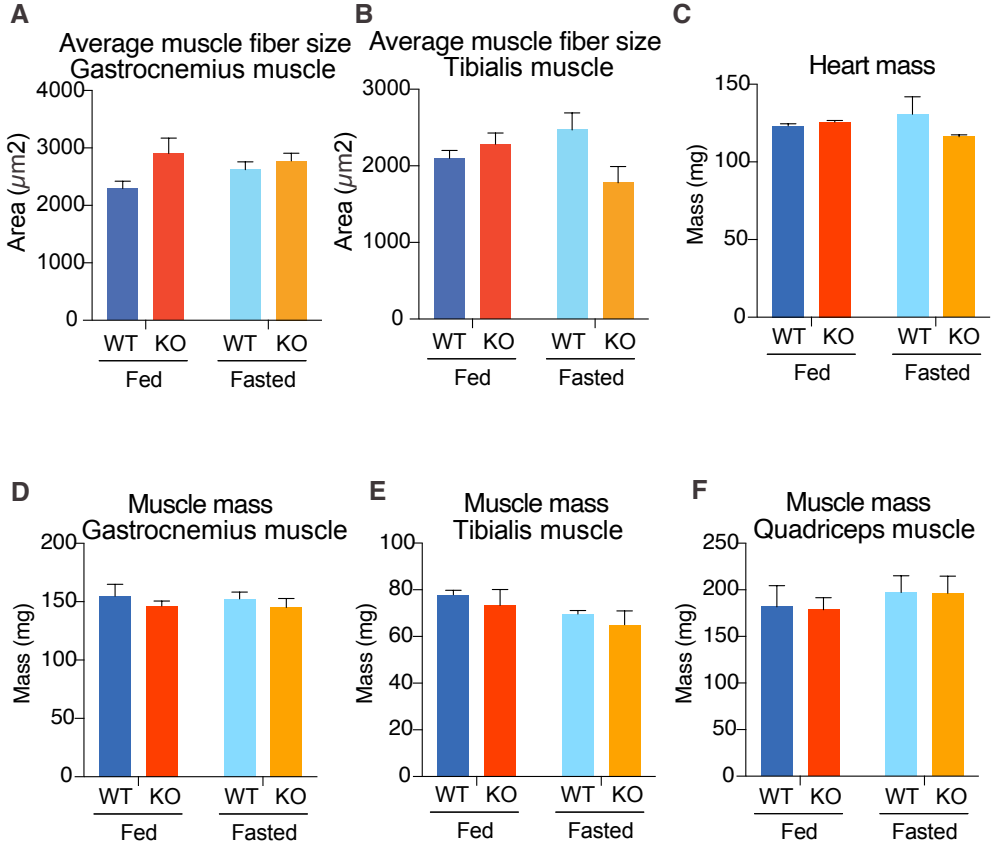
Figure 3—supplement 2